Journal of Drug Delivery Science and Technology 100 (2024) 105995

Contents lists available at ScienceDirect

Journal of Drug Delivery Science and Technology

journal homepage: www.elsevier.com/locate/jddst

Experimental design and characterization of dual-antibody-conjugated all-trans retinoic acid-loaded lipid nanoparticles as a potential cancer therapy

Zeynep Islek [a,b], Ali Asram Sagiroglu [c,d], Mehmet Hikmet Ucisik [b], Oguz Kaan Kirbas [b], Erhan Demirel [e], Aysu Yurdasiper [a], Fikrettin Sahin [b], Ozgen Ozer [a,*]

[a] Department of Pharmaceutical Technology, Faculty of Pharmacy, Ege University, Erzene, 35040, Bornova, Izmir, Turkiye
[b] Department of Genetics and Bioengineering, Faculty of Engineering, Yeditepe University, İnönü Mh., Kayışdağı Cd. No: 326A, 34755, Ataşehir, Istanbul, Turkiye
[c] Department of Pharmaceutical Technology, Faculty of Pharmacy, Istanbul University-Cerrahpasa, 34500, Istanbul, Turkiye
[d] Department of Pharmaceutical Technology, Faculty of Pharmacy, Bezmialem Vakif University, Fatih, Istanbul, Turkiye
[e] School of Engineering and Natural Sciences, Department of Biomedical Engineering, Istanbul Medipol University, Kavacık Mah, Ekinciler Cad. No: 19, Kavacık Kavşağı, 34810, Beykoz, Istanbul, Turkiye

ARTICLE INFO

Keywords:
Solid lipid nanoparticles (SLNs)
Anti-programmed death-ligand 1 (anti-PD-L1)
All-trans retinoic acid (ATRA)
Anti-4-1BB
Antibody conjugation
Surface modification

ABSTRACT

Antibody-targeted immunotherapy has emerged in cancer therapies regarding checkpoint inhibition with monoclonal antibodies, such as anti-programmed death-ligand 1 (anti-PD-L1) either given alone or in combination. However, when given alone, it may fail to activate tumor-specific T cells. The combinational therapy of anti-PD-L1 with anti-4-1BB and all-trans retinoic acid (ATRA) has come into prominence due to disease heterogeneity, resulting in the synergistic effects associated with greater T-cell responses. This study introduces anti-PD-L1 and anti-4-1BB-conjugated ATRA-loaded solid lipid nanoparticles (SLNs), where the Design-Expert Program was applied for the optimization. Accordingly, antibody–conjugated ATRA-loaded SLNs had uniform dispersions with mean diameters of 179.6 ± 12.6 nm. The formulations achieved the encapsulation efficiency (EE %) of ATRA at 21.2 ± 1.4 %, regarding the three-dimensional response surface graph. The binding efficiency of anti-4-1BB and anti-PD-L1 antibodies were determined as 85.59 ± 7.3 % and 90.02 ± 5.4 %, respectively. The release profile of formulations indicated the biphasic release of ATRA (*ie*., 76 ± 4.4 %) from SLNs within 24 h via the Higuchi model. Particle size distributions of SLNs displayed a 7 % increase (i.e., 190.5 ± 7.63 nm) at 4 °C over 2 months. The experimental design of anti-PD-L1- and anti-4-1BB-conjugated- ATRA-loaded SLNs highlighted the promising strategy for the development of alternative formulations and the potential approach for further cancer therapies.

1. Introduction

Antibody-targeted immunotherapy has emerged as a significant breakthrough in the field of oncology in recent years [1–3]. Numerous investigations in various tumor types have shown that among immunotherapies, checkpoint blockade constitutes a major step forward considering the efficacy of results in patients with checkpoint inhibitors, including as an anti-Programmed Death-1 (anti-PD-1), across a wide spectrum of cancer types (e.g., melanoma, small cell lung cancer) when given in alone or in combinational therapy [1–3]. The recent research on the immune checkpoint blockade by using monoclonal antibodies (mAbs), including anti-PD-L1, revealed that they indicated a significant role in the immune system, and suggested that checkpoint inhibition might delay tumor growth and decrease metastasis by activating T cells [4]. Moreover, this blockade can enhance survival, and reverse exhaustion of the immune cells, particularly in $CD4^{+}$T that are specific for tumor antigens, as previously reported in murine melanoma models [5,6].

Although PD-1/PD-L1 blockade is clinically verified in cancer immunotherapy, it may not be sufficient to fully activate tumor-specific T cells. The previous study indicated that the dual therapy of anti-PD-L1 with the co-stimulatory receptor 4-1BB (CD137) co-therapy increases the checkpoint inhibition of PD-1 synergistically in mouse models [5, 7–9]. Part of the synergy stems from the fact that a subset of

* Corresponding author.
E-mail address: ozgen.ozer@ege.edu.tr (O. Ozer).

https://doi.org/10.1016/j.jddst.2024.105995
Received 25 January 2024; Received in revised form 19 July 2024; Accepted 25 July 2024
Available online 30 July 2024

tumor-infiltrating T lymphocytes expresses both PD-1 and CD137 on their surface, resulting in a combinational efficacy on T cells that is extremely noticeable even in relatively low immunogenic mice cancer models [8]. In addition, the anti-cancer effects of anti-PD-L1 appear to be enhanced by combination therapy methods, which are co-administered with an active pharmacological agent. Among the active molecules in combination with anti-PD-L1, all-trans retinoic acid (ATRA), which is the oxidized carboxylic acid form of all-trans-retinol, was reported to improve the efficacy of anti-PD-L1 in cervical cancer regarding the inhibition of myeloid-derived suppressive cell (MDSC) function [10]. Recently suggested that a combination of anti-PD-L1 and ATRA may induce the maturation of MDSC related to the resistance to anti-PD-1 therapies and target the resistance mechanism to improve the efficacy of anti-PD-1 based immunotherapy [11]. On the other hand, PD-L1 inhibitors can lack the ability to specifically target tumors [12]. As a result, the inability to effectively use these inhibitors can be attributed, to some extent, to the unavoidable systemic immune toxicity, off-target effects, and occasionally high healthcare expenses [13,14]. To overcome these drawbacks, there is a crucial need for the targeted and effective delivery systems (i.e., polymeric nanoparticles, liposome, SLN, etc.) of these newly designed PD-L1 blockers to enhance the sensitivity of PD-L1-targeting malignancy therapy [12].

In a similar manner, despite the promising anticancer effects of ATRA, the low aqueous solubility (logP = 6.6) and its high toxicity, targeted drug delivery systems (DDS) accompanied by the administration of ATRA in a nanocarrier system have been considered as a promising strategy to address drawbacks and bioavailability [15,16]. Delivery of ATRA within DDS, including solid lipid nanoparticles (SLN) reduces the toxicity and enhances the therapeutical efficacy. Previously, polymeric nanoparticles including poly (lactide-co-glycolide acid) (PLGA)-poly (ethylene glycol) (PEG) (PLA–PEG) have been used to synthesize nanoparticular systems of ATRA loading with enriched characteristics due to the hydrophilic nature, low toxicity, and biocompatible properties of PEG [17]. Incorporation of ATRA into nanoparticles, leads to an increase in the efficacy of transfer of compounds into the cancer cells, thereby decreasing the interaction with the healthy cell membrane, and reducing toxicity by gaining the “stealth” characteristics of the nanoparticles with the pegylation strategy, thus resulting in decreasing the opsonization process and clearance by the mononuclear phagocyte system (MPS), and enhancing the prolonged circulation time of the nanoparticle in the bloodstream [18]. Similarly, on the active drug targeting strategy, anti-PD-L1-conjugated and ATRA-loaded nanoparticles improved immunotherapeutic activity in oral dysplasia and oral squamous cell carcinoma with fast cellular uptake [17]. In addition, anti-PD-L1 and anti-4-1BB- conjugated iron-dextran particles were developed by Kosmides et al. (2017) to inhibit checkpoint PD-L1 signal and activate T cells through the 4-1BB co-stimulation for the delay on tumor survival [19]. Moreover, Moon et al. indicated that the anti-PD-L1 and a cathepsin B-specific cleavable peptides were conjugated to doxorubicin (DOX) molecule, resulting in the formation of prodrug nanoparticles, and targeted tumor delivery with minimal side effects by combining PD-L1 blockade and immune checkpoint blockade in breast tumor models [20].

With this targeted delivery approach, nanoparticles with the potential to be employed as efficient and specific drug delivery methods have shown promise in addressing the issues of freely available medicinal substances [13,21]. Currently, nanoparticles have gained attention for their advantageous properties such as active or passive targeting of tumors, enhanced tissue accumulation and cellular uptake, favorable permeability through biological barriers, and controlled release of drugs or payloads. Therefore, a wide range of nanoparticles such as solid lipid nanoparticles have been identified, which have received approval from the Food and Drug Administration (FDA) [12,22]. In addition to this, numerous clinical trials are currently investigating a wide range of disease treatments or diagnosis procedures that utilize nanoparticles [22,23]. In tumor therapy, a diverse range of nanoparticles have been specifically engineered to transport different PD-L1 inhibitors, including PD-L1 antibodies, targeted delivery systems, small molecule inhibitors, and nucleic acids like miRNA, siRNA, and CRISPR systems [24].

Likewise, this study presents an alternative solid lipid-based DDS, for the PD-1 targeted delivery of ATRA to cancer cells thereafter for future studies. Tripalmitin-based SLNs are synthesized as nanocarrier vesicular systems, consisting of multiple layers of phospholipids surrounding a solid fat [21–23]. Like liposomes and emulsomes, the outermost structure of SLNs is allowed to be stabilized by phospholipid layers and pegylated by using maleimide-containing PEGylated phospholipid 1, 2-distearoyl-sn-glycero-3-phosphoethanolamine-N-[maleimide-2000] (DSPE-PEG_{2000}-Maleimide), and thus eliminating the need for surfactants to provide the biocompatibility [21,24]. In addition, these system benefits from key properties of the solid- or crystalline-state fat, including, (i) a high drug loading capacity for the lipophilic compounds in which the lipid-based cargo can be found in both the phospholipid (PL) layers and the solid fat core, (ii) a prolonged release of the drug compounds from the solid matrix [21–23], (iii) a lipid-based and surfactant-free drug delivery system for several lipophilic compounds on various cancer cells and (iv) biocompatibility, and biodegradability [25–29]. Taking advantage of these features, in this study, SLNs were proposed as the potential alternative therapy for the delivery of poorly water-soluble therapeutic agents such as ATRA, and the development of targeted immunotherapeutic formulations by the conjugation of anti-PD-L1 and anti-4-1BB mAbs to SLNs.

In the fields of DDS including, polymeric drug conjugates and antibody-targeted systems, the maleimide-thiol process has become increasingly prominent in surface modification and DDS functionalization [30–34]. In line with this approach, maleimides can lead to stable thioether linkages forming when they interact with thiols, which can be explained by their selectivity to thiols, rapid aqueous reaction rates, and moderate reaction conditions [35,36]. Considering previous studies, two commonly used functionalization techniques for nanoparticles were used for the SLN surface modification to improve the conjugation capacity of the mAbs to DSPE-PEG-maleimide modified SLNs: (i) the addition of DSPE-PEG_{2000}- Maleimide during the preparation of SLNs by film hydration and (ii) post-insertion after SLN formation [37,38].

With this approach, overall, this study aims to design an alternative solid lipid-based DDS for the PD-1 targeted delivery of ATRA-loaded lipid-based nanocarriers, their structure, and associated features including the production methods, characterization studies, and stability. The present study introduces the alternative formulation strategy of anti-PD-L1 and anti-4-1BB-conjugated ATRA-loaded SLNs. The ATRA-loaded SLNs were synthesized by using the Design-Expert Program, and the functionalization of SLNs was achieved with the DSPE-PEG-maleimide group onto the surface of the nanoparticles. For the surface modification of SLNs, anti-PD-L1 and anti-4-1BB mAbs were thiolated, and directly conjugated to the amide group of DSPE-PEG-maleimide, and thus the maleimide (Mal) end of DSPE-PEG-maleimide were attached to the sulfhydryl (-SH) groups of thiolated anti-PD-L1 and anti-4-1BB mAbs. Subsequently, the characterization studies of the SLN formulations were examined including, physicochemical and morphological analysis, protein detection by Sodium Dodecyl Sulfate-Polyacrylamide Gel Electrophoresis (SDS-PAGE) Analysis, Bradford assay, and flow cytometry analysis for the confirmation of antibody conjugation to SLNs, whereas the physical stabilities of the formulations in both a semi-liquid and lyophilized state after surface modification were also tested throughout the study.

2. Material and methods

2.1. Materials

ATRA, glyceryl tripalmitate (tripalmitin, purity ≥99 %), and cholesterol (≥99 %) were obtained from Sigma-Aldrich, Germany. DSPE-PEG_{2000} Maleimide (ammonium salt) and DSPE-PEG_{2000} Amine

were obtained from Avanti Polar Lipids (Birmingham, AL). Chloroform (≥99.8 %) was purchased from Fluka Chemika, Germany. Anti-IgG (whole molecule) and Anti-PD-L1 (clone 10F.9G2) were purchased from Sigma-Aldrich, Germany, and Anti-PD-L1 (FITC) antibodies were obtained from Abcam, United Kingdom. Clone 3H3, Anti-Mouse CD137 (4-1BB) were purchased from Leinco Technologies and PE anti-mouse CD137 (4-1BB) Antibodies were obtained from Biolegend, USA. Pierce Traut's Reagent (2-iminothiolane) and DTNB (Ellman's Reagent) (5,5-dithio-bis-(2-nitrobenzoic acid) were obtained from ThermoFisher Scientific, USA.

2.2. Preparation of ATRA-loaded and dual antibody-conjugated SLNs

2.2.1. Synthesis of ATRA-loaded, maleimide-functionalized PEGylated SLNs

Empty and ATRA-loaded PEGylated SLNs have been synthesized by the film hydration method described before with slight modifications [26,27]. Briefly, ATRA and lipids including sphingomyelin and tripalmitin together with cholesterol, DSPE-PEG_{2000}-Amine, and DSPE--PEG_{2000}-Maleimide were dissolved in chloroform (2 mL) at a molar ratio of 2:1:0.08:0.02 [26,39]. The ratio of total Phospholipid (Ph): Tripalmitin (Tri) was kept constant in the range of 0.1–0.15 (w/w). The solvent was entirely removed and rehydrated with an aqueous solution. Particles were homogenized by ultrasonication at 65 °C for 50 min. Using the post-insertion method, SLNs were mixed with DSPE-PEG-Maleimide at a ratio of 1:1 (w/v) overnight and the following day, SLNs modified with PEG-Maleimide were obtained by centrifugation at 14,000 g for 30 min. The pH values of the obtained formulations were measured (n = 3) after each synthesis.

2.2.2. Experimental design of ATRA-loaded, maleimide-functionalized PEGylated SLNs

The optimization of ATRA-loaded PEGylated SLN formulation was achieved by the response surface methodology as previously described in Sagiroglu et al. [40]. Accordingly, tripalmitin and ATRA were selected as the critical components for the optimization of SLN formulation where the ratios of ATRA: Tripalmitin (Tri) and Phospholipid (Ph): Tripalmitin (Tri) were kept constant at 0.10–0.15 (w/w, %) and 0.05–0.2 (w/w, %), respectively [41,42]. The Central Composite Design (CCD) was used to investigate the impact of two independent factors on the formulation of SLN across five different levels, which were represented as -α, −1, 0, +1, and +α. To ensure that the design was both rotatable and orthogonal, a value of 1.41 was selected. Regarding the selected parameter, SLN formulation was synthesized using various amounts of ATRA (2.17–7.83 mg) and Tri (37.17–42.83 mg). 13 experiments were carried out to attain precision, presented in Table 1.

The response variables, which are the critical parameters for the optimization of the formulation, were selected as Particle Size (PS), Polydispersity Index (PDI), and % Encapsulation Efficiency (% EE). To improve the efficiency of experimental design and analysis, the Design-Expert software (version 10.0.3.0) was employed, and the obtained response was assessed using a quadratic polynomial equation.

$$Y: \beta_0 + \beta_1 A + \beta_2 B + \beta_{12} AB + \beta_{11} A^2 + \beta_{22} B^2$$

Accordingly, *Y* was abbreviated as predicted (pred.) response; A and B were independent variables; A^2 and B^2 represented the interaction and quadratic terms, respectively; β_0 represented the intercept value; β_1 and β_2 were the abbreviations of the linear coefficients; β_{12} represented the interaction coefficient; β_{11} and β_{22} were the quadratic coefficients.

The study evaluated the influences on responses by independent variables using analysis of variance (ANOVA). The model's suitability and accuracy were evaluated by computing the pred. and adjusted (adj.) R^2. The utilization of three-dimensional (3D) surface graphics was employed to visually represent the experimental region and the impact of independent variables on the response, and the pred. and adj. R^2 was calculated. The optimal formulation was determined by considering the maximum EE (%) and the lowest PS and PDI values, and the outcomes were contrasted with the expected values.

Table 1
Variables in CCD.

Variables		Level of variables				
		−1.41	−1	0	1	1.41
A	ATRA (mg)	2.17	3	5	7	7.83
B	Tri (mg)	37.17	38	40	42	42.83

2.2.3. Thiolation of antibodies: quantification of thiol groups

Immunoglobulin G (IgG) antibody was used in the optimization of antibody thiolation. Anti-IgG (1 mg/mL) was diluted 1:10 in PBS (pH = 8) containing DTT (Dithiothreitol) (5 mM), and EDTA (Ethylenediamine tetraacetic acid) (5 mM). Subsequently, diluted anti-IgG was incubated with Traut's Reagent (2-iminothiolane solution) (5.7 mg, in 5.0 mL phosphate buffer, pH 8.0) at a ratio of 50:1 for 2 h, on a magnetic stirrer, under argon gas, at 20 °C ambient temperature [31]. The thiolated antibody was subsequently purified by ultracentrifugation (Amicon Ultra-0.5 Centrifugal Filter Unit, 30 kDa, Millipore). Thiolation of anti-4-1BB (100 μg/mL) and anti-PD-L1 (100 μg/mL) mAbs was performed using the same procedure with a slight modification of anti-IgG antibody thiolation, and ultracentrifuge filters (Amicon Ultra-0.5 Centrifugal Filter Unit, 10 kDa, Millipore) were selected as the molecular weight cut-off (MWCO). The efficiency of thiolation together with the amount of thiol groups in the antibody was quantified photometrically by means of Ellman's reagent (5, 5′ dithiobis-(2-nitrobenzoic acid) or (DTNB) at 412 nm, regarding quantitating sulfhydryl groups based on molar absorptivity as described in the manufacturer's protocol. The amount of thiol groups was calculated in relation to L-cysteine standard solutions handled to determine the antibody quantification and then, the concentrations of sulfhydryl groups per thiolated anti-IgG (1 mg/mL), thiolated-anti-4-1BB (100 μg/mL) and thiolated-anti-PD-L1 (100 μg/mL) were calculated.

2.2.4. Preparation of dual antibody-conjugated SLNs

The optimized empty/ATRA-loaded PEGylated (DSPE-PEG-Maleimide-modified) SLN was conjugated with thiolated antibodies through the binding of the maleimide (Mal) end group of DSPE-PEG-maleimide to the –SH groups of thiolated anti-PD-L1 (clone 10F.9G2) and thiolated anti-4-1BB (clone 3H3) monoclonal antibodies. The antibody conjugation of SLN was accomplished by modifying the procedure described by Steinhauser and colleagues [43]. Accordingly, the thiolated (i) anti-IgG, (ii) anti-PD-L1, (iii) anti-4-1BB, and (iv) both anti-PD-L1 and anti-4-1BB antibodies were conjugated to the optimized empty/ATRA-loaded PEGylated SLNs. Briefly, thiolated antibodies were allowed to bind to ATRA-loaded PEGylated SLN at a ratio of 1:1 (v/v) for at least 12 h, in a magnetic stirrer, under argon gas at 20 °C ambient temperature. The unbound antibody was then separated by centrifugation and washing 3 times with PBS (pH = 7.2).

2.2.5. Lyophilization of ATRA-loaded PEGylated SLNs

The optimized ATRA-loaded PEGylated SLN formulations were first frozen at −20 °C for 12 h with cryoprotectant (trehalose) and then, they were dried for 24 h at −65 °C under a vacuum of 0.005 mbar hPa, as previously described by our colleagues [32]. Accordingly, the lyophilized SLNs were dispersed in distilled water at room temperature in a shaker. Then, SLN formulations were analyzed using Zetasizer, and SEM in terms of PS distributions.

2.3. Characterization studies of SLNs

2.3.1. Physicochemical parameters: PS, PDI, particle concentrations, and zeta-potential

The mean PS, PDI, and the mean zeta potential (ZP) of SLN formulations were measured by the dynamic light scattering (DLS) method at 25 °C using a Zetasizer (Malvern Instruments Ltd, UK), after dilutions with distilled water to handle proper concentrations. In addition, the particle concentration of SLN formulations was determined using a Nanoparticle Tracking Analysis (NTA) (NanoSight NS300, Malvern), as previously described by our colleagues [27]. Video capture was analyzed on NTA software version 3.4. All findings were calculated as the mean of measurements and samplings in triplicate for each formulation.

2.3.2. Morphological evaluation by scanning electron microscopy (SEM)

The optimum empty and ATRA-loaded PEGylated SLN formulations were morphologically analyzed using an SEM (Zeiss EVO-HD-15). Before imaging, a short-term fixation method was applied [27], and the samples were examined under SEM after gold sputtering (EM ACE200, Leica).

2.4. Determination of PEGylation and surface modification: nuclear magnetic resonance (NMR) spectroscopy, and fourier-transform infrared spectroscopy (FTIR) analysis

Hydrogen NMR (^{1}H NMR) and the FTIR spectra of DSPE-PEG-Maleimide-modified SLN formulations were investigated to determine the PEGylation and surface modification. Briefly, ^{1}H NMR (500 MHz) spectra were measured in $CDCl_3$ using an Agilent VNMRS 500 MHz instrument. $Si(CH_3)_4$ was used as an internal standard. Samples were lyophilized and the resulting lyophilized samples were dissolved in $CDCl_3$, filtered, and transferred to NMR tubes.

Together with the ^{1}H NMR, FTIR spectra of ATRA, DSPE-PEG_{2000}-Maleimide, and ATRA-loaded-DSPE-PEG_{2000}-Maleimide - modified SLN formulations were recorded from 4000 cm^{-1} to 650 cm^{-1} using the FTIR spectrometer. Measurements were performed in triplicate.

2.4.1. Differential scanning calorimetry (DSC) analysis

The optimized empty and ATRA-loaded PEGylated SLNs were investigated by a DSC (PerkinElmer DSC-8000), as previously described in Ref. [33]. Accordingly, the samples were first hydrated with water, and analyzed using DSC analysis under 20 mL/min nitrogen flow in a range from 20 °C to 250 °C at a heat rate of 10 °C/min.

2.4.2. SDS-PAGE analysis

Protein characterization was performed using the SDS-PAGE method to detect the conjugation of mAbs to SLNs. Gels were used at 12 % concentration according to the size of anti-PD-L1 and anti-4-1BB monoclonal antibodies. Since the sizes of both antibodies are close to each other (anti-PD-L1: 32.78 kDa, anti-4-1BB: 39 kDa), separate gels were prepared for each antibody. Accordingly, the samples of antibody-conjugated SLNs (20 μl), 2-Mercaptoethanol (5 %), Bromophenol blue (0.01 %), Glycerol (10 %), SDS (2 %), and Tris-HCl were suspended in 4X Laemmli buffer and was left at 95 °C in a heat block for 5 min. Afterward, 20 μg of protein sample was loaded into each well of the gel and run by applying 90V for 15 min and 120V for 75 min. Gel images were visualized with the ChemidocTM XRS + system.

2.4.3. Bradford Assay

The Bradford assay test was used to determine the concentration of antibodies conjugated to SLNs. According to the Bradford protein test protocol, BSA standards were prepared in the concentration range of 5–100 μg, and the amount of antibody conjugated to nanoparticles was determined according to the polynomial graph. The protein concentration of bounded/unbounded antibodies (remaining in the supernatant) was measured by Bradford protein assay and the binding efficiency (%) was calculated according to the following equation:

$$\text{Binding Efficiency } (\%) = \frac{\text{Wtotal} - \text{WAb in the supernatant}}{\text{Wtotal}} \text{ x } 100\ \%$$

$W_{\text{total Ab}}$: Total amount of antibody; $W_{\text{Ab in the supernatant:}}$ The amount of antibody remaining in the supernatant.

2.4.4. Flow cytometry analysis

The amounts of mAbs per nanoparticle were determined using the fluorescently labeled antibodies by flow cytometer. Accordingly, Phytoerythrin (PE) labeled-anti-4-1BB (Biolegend) and Fluorescent Isothiocyanate (FITC) labeled-anti-PD-L1 (Abcam) mAbs (1:1 (v/v ratio)) were conjugated to the optimized empty and ATRA-loaded PEGylated SLNs. Antibody concentration was measured by flow cytometry at FL1 and FL2 filters with regard to the excitation (PE at 566 nm; FITC at 491 nm) and emission (for PE at 574 nm; FITC at 516 nm). Three independent experiment sets were performed. It was statistically interpreted on GraphPad Prism Software (version 8.01) by a Two-way ANOVA.

2.4.5. Analytical quantification of ATRA encapsulated in SLNs

The quantification of ATRA encapsulated within SLN was determined by the reversed-phase high-pressure liquid chromatography (RP-HPLC) (Shimadzu SPD-20A). Accordingly, ultrapure water was employed as the mobile phase with filtered and degassed acetonitrile (80:20, v/v). The mobile phase was introduced at a flow rate of 1 mL/min through the InertSustain C18 column (150 × 4.6 mm, 5 μm) kept at a constant temperature of 25 °C, and the UV analysis was read out at 352 nm.

Following the dilution of ATRA stock solution with acetonitrile was prepared for the linearity analysis. Peak area and ATRA concentrations between 0.05 and 20 μg/mL were linearly associated ($r^2 = 0.9996$). The samples prepared with free SLNs and formulations with ATRA-loaded PEGylated SLNs did not indicate any interaction with ATRA peaks, demonstrating the method's selectivity, accuracy, and precision.

2.4.6. Encapsulation efficiency (EE (%))

The encapsulation efficiency of SLNs was determined using the ultracentrifuge method. Accordingly, the samples were ultracentrifuged at 14,000 rpm for 30 min, and ATRA-loaded solid lipid nanoparticles were precipitated and the remaining supernatant (containing the free lipids and drugs) was taken and filtered through 0.2 μm filter paper. After dilution with Acetonitrile: PBS (80:20), the samples were measured in the previously validated RP-HPLC method, and the calculation of EE % for ATRA-loaded PEGylated SLNs was performed using the following equation:

$$\text{EE } (\%) = \frac{\text{Wincorporated compound}}{\text{Wtotal}} \text{ x } 100\%$$

$W_{\text{incorporated compound}}$: the amount of ATRA in the SLNs; W_{total}: the amount of ATRA used in the formulation.

2.4.7. In vitro drug release from SLNs

In vitro releases of the optimized nanoparticle formulations were performed with the dialysis bag method as previously described in Sagiroglu et al. [40]. Briefly, 1 mL of ATRA-loaded SLN formulations were placed in the cellulose acetate membrane dialysis bag (molecular weight cut off 12–14 kDa, Spectra/Por®, Canada) sealed, and then, these bags were submerged in 150 mL of PBS: Ethanol (20:80; pH 7.4) mixture in a beaker. They were placed on a shaking incubator at 37 ± 0.5 °C and 400 rpm/min, and the whole system was covered with aluminum foil to avoid UV light exposure. Samples were taken from the receptor phase at certain time intervals, including 0, 0.15, 0.3, 0.45, 1, 2, 3, 4, 8, and 24 h, and changed with a fresh solution at an equivalent volume to ensure sink conditions. Using the validated HPLC method, the

amount of ATRA released from SLNs was determined cumulatively. The kinetic mechanisms of ATRA release from SLN formulations were established using mathematical models, including zero-, and first-order, Higuchi root-square, and Hixson-Crowell regarding their coefficients (r^2). Accordingly, C was abbreviated as drug concentration released at pre-determined time (t); C_0: represented as initial ATRA concentration; k_0, k_1, and k_2 were abbreviated as zero-order, first-order, and Higuchi release rate constants, respectively. W_0 and W_t are represented as initial drug quantity in the formulation, and the amount of drug remaining in the formulation at the time (t), respectively. k_H was a constant that incorporated the relation of the surface and volume. Accordingly, $C = k_0t + C_0$ (Zero-order); $\text{In } C = \text{In } C_0 + k_1t$ (First-order); $C = k_2t^{½}$ (Higuchi model); $W_0^{1/3} - Wt^{1/3} = k_H$ (Hixson–Crowell)

2.5. Stability studies

To examine the stability of the formulations, empty and ATRA-loaded PEGylated SLNs were stored at 4 ± 1 °C in the refrigerator, 25 ± 2 °C (60 % relative humidity), and 40 ± 2 °C (75 % relative humidity) for 9 months at day 0, 15, 30 (1 month), 45, 60 (2 months), 150 (5 months), 210 (7 months) and 270 (9 months) in the stability cabinets. Stability studies of anti-PD-L1-anti-4-1BB conjugated-ATRA-loaded SLN formulations were performed under the same conditions for 2 months.

The physical appearance of formulations, and alterations in properties such as pH, ZP, and size according to the months were evaluated. All formulations containing ATRA were stored in the dark. The experiments were performed with three independent studies.

2.6. Statistical analysis

The statistical analysis was conducted utilizing GraphPad Prism Software (version 8.01). The error bars in the graph represent the mean standard errors. The statistical analysis involved the use of ordinary one-way ANOVA and two-way ANOVA, followed by a post hoc Tukey's multiple comparison test to compare the data sets. The unpaired *t*-test was employed for a two-group comparison involving an individual. Statistical significance was determined based on the following criteria: (ns) $P \geq 0.05$, (*) $P \leq 0.05$, (**) $P \leq 0.01$, (***) $P \leq 0.001$, and (****) $P \leq 0.0001$. Data represents the mean ± SD of at least 3 independent experiments.

3. Results and discussions

In therapeutic applications for intradermal/intravenous routes of administration, SLNs stabilized with phospholipids and cholesterol do not need surface active agents as stabilizing agents when using the film hydration method, providing them with high biocompatibility. Similar to liposomes, SLNs could be modified with proteins, ligands, polymers, or antibodies to meet specific requirements, such as extended blood circulation and targeted drug delivery.

3.1. Experimental design of SLN formulations

CCD setup and the responses from 13 experiments are illustrated in Fig. 1, and Table 2, displays the 3D response surface graphs pertaining to the statistically significant variables of PS, PDI, and EE (%) on the

Table 2
CCD matrix and responses.

Run	Variables		Responses		
	A: ATRA	B: Tri	PS (nm)	PDI	EE (%)
1	3	42	170.2	0.382	14.5
2	3	38	173.4	0.235	8.6
3	7	38	208.4	0.341	28.4
4	5	37.1	199.5	0.236	26
5	5	42.8	208.2	0.362	30
6	7.8	40	210.6	0.35	28.4
7	7	42	207.8	0.309	25.4
8	5	40	165.3	0.278	19.1
9	5	40	179.6	0.235	22.3
10	5	40	175	0.24	20.2
11	5	40	176.7	0.222	18.5
12	5	40	178.2	0.255	20.6
13	2.2	40	164	0.344	6

Abbreviations: ATRA, All-trans Retinoic Acid; Tri, Tripalmitin.

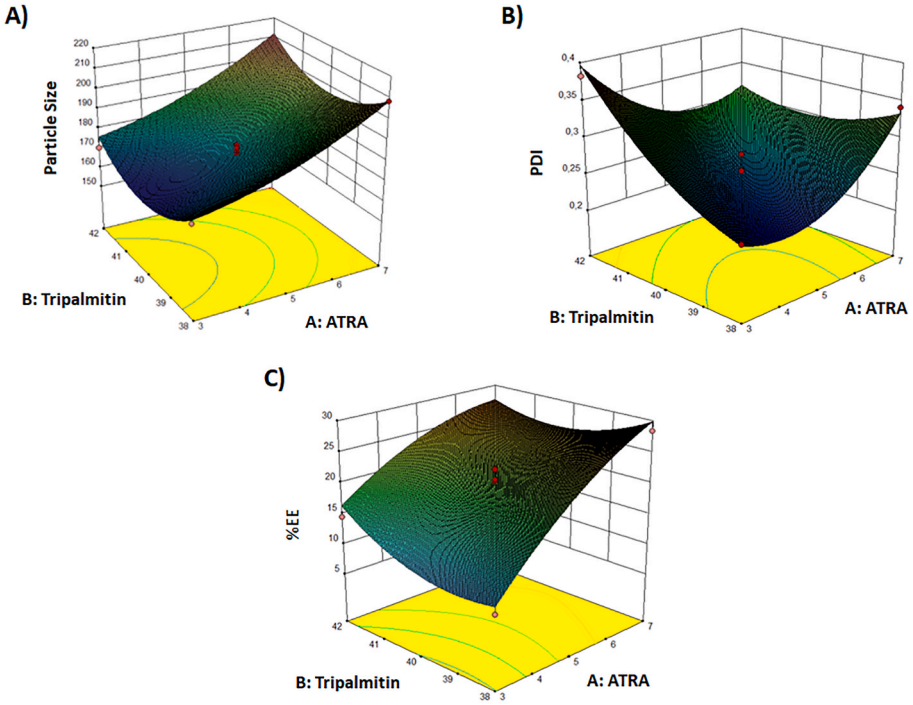

Fig. 1. 3D-response surface plots of SLN formulations for **(A)** PS distribution, **(B)** PDI, and **(C)** EE (%).

critical parameters. The polynomial equations generated by the Design-Expert Software have unveiled the discrete primary and interactional impacts of the independent variables on the corresponding dependent variables during the analysis.

The selection of the CCD model for the design of SLNs involves the criteria to optimize the formulation process and achieve the desired characteristics of the nanoparticles. Some common criteria considered as (i) Factorial Screening: CCD is often chosen for its ability to screen multiple factors simultaneously efficiently. In the case of SLNs, factors such as lipid type, surfactant concentration, and drug loading may be screened to identify significant variables affecting nanoparticle properties, (ii) Response Surface Optimization: CCD allows for response surface optimization, enabling researchers to determine the optimal levels of formulation variables to achieve desired nanoparticle characteristics, which includes factors such as particle size, polydispersity index (PDI), drug encapsulation efficiency, and stability, (iii) Experimental Efficiency: CCD designs are efficient in terms of the number of experimental runs required to estimate main effects, interactions, and quadratic effects. This efficiency is valuable in the context of SLN formulation optimization, as it minimizes the number of experiments needed while still providing robust results, (iv) Model Fitting and Predictability: CCD models are typically good at fitting nonlinear response surfaces, which is advantageous when dealing with complex relationships between formulation factors and nanoparticle properties, thus allowing for accurate prediction of nanoparticle characteristics based on the chosen formulation parameters, (v) Robustness Analysis: CCD designs facilitate robustness analysis, helping researchers assess the sensitivity of the optimized formulation to small variations in the experimental conditions or formulation variables, (vi) Statistical Analysis: CCD models enable statistical analysis of the experimental data, allowing researchers to determine the significance of factors, identify interactions, and assess model adequacy, (vii) Versatility: CCD can accommodate both categorical and continuous factors, making it versatile for SLN formulation studies where various types of factors (e.g., lipid type, surfactant concentration, and processing parameters) may need to be considered. Accordingly, optimization of the ATRA-loaded SLN formulation was performed using response surface methodology. The criteria were selected according to the previous studies and literature [40,44]. The amounts of tripalmitin and ATRA were determined as factors used for optimization in the formulation and the molarity ratio of Phospholipid: Tripalmitin is (in the range of 0.10–0.15), and the ratio of ATRA: Tripalmitin is (0.05–0.2) (w/w) ratio) was kept constant in the system.

3.1.1. The impact of independent variables on the PS

The design matrix revealed that the size of SLNs exhibited significant variation, ranging from 164 to 210.6 nm (Table 2). The minimum PS was calculated according to the quadratic equation as follows:

$$\textbf{PS}: 174.96 + 17.31A + 1.06B + 0.65AB + 4.76A^2 + 13.04B^2$$

Table 3 displayed the ANOVA analysis of the regression model for PS, which was evaluated using the PS equation. The statistical analysis indicated that the model equation was highly significant ($p < 0.0001$), as evidenced by the high F value (22.30) and low P-value (<0.001) (Table 3). Furthermore, the lack of fit value (1.05) was found to be statistically insignificant ($p = 0.4615$), indicating that the model fits well. The coefficient of determination (R^2) with a value of 0.9409 suggests that the model was successful in elucidating 94.09 % of the total range of possible responses to the experimental conditions.

The pred.R^2 value of 0.7631 was consistent with the adj. R^2 value of 0.8987, indicating a correlation between measured and predicted values. These findings indicated that an increase in the amount of ATRA ($p < 0.05$) had a considerable impact on the PS of nanoparticles, compared to that in Tripalmitin ($p > 0.05$). In addition, the 3D response surface plot verified that there was a direct relationship between the amount of ATRA and the enlargement of PS.

Many parameters can affect the physicochemical properties, including the amount of phospholipids, cholesterol, and tripalmitin within SLN formulation. The molar ratios of lipids, including sphingomyelin, cholesterol, mPEG2000-DSPE and DSPE-PEG2000-Maleimide added to the formulation were determined as 2:1:0.08:0.02, according to previous studies [26,27,39], where the Phospholipid: Tripalmitin ratio is a significant factor in determining both the size and the stability of SLN formulations [45]. The ratio should be in the range of 0.1–0.5; otherwise, particle stability may not be maintained due to the by-product formation [41,42]. In the previous study, it was revealed that an increase in the Phospholipid: Tripalmitin ratio in the range of 0.14–0.4 resulted in an increase in the size of SLNs, and hence an improved entrapment efficiency of the drug-loaded to SLNs [42,46]. Although the increase in PS was linked to the increase in the phospholipid bilayer, a definite relationship between the amount of phospholipid and the size of the particle could not be established [42,46]. Besides, in our study, the Phospholipid: Tripalmitin ratio was optimized as 0.12, which is consistent with the literature [41]. In addition, it has been shown in the literature that the combined use of sphingomyelin and cholesterol increases *in vitro* stability and *in vivo* biological activity compared to DSPC/cholesterol [47]. In line with these parameters and methodology, the synthesis of optimum empty PEGylated SLN formulation was achieved by the film hydration.

Table 3
ANOVA values for PS.

Source	Sum of Squares	df	Mean Square	F Value	p-value Prob > F	
Model	3657.66	5	731.53	22.30	0.0004	Significant
A-ATRA	2397.86	1	2397.86	73.08	<0.0001	
B-Tri	9.04	1	9.04	0.28	0.6159	
AB	1.69	1	1.69	0.052	0.8269	
A^2	157.87	1	157.87	4.81	0.0643	
B^2	1182.67	1	1182.67	36.05	0.0005	
Residual	229.68	7	32.81			
Lack of Fit	101.30	3	33.77	1.05	0.4615	not significant
Pure Error	128.37	4	32.09			
Cor Total	3887.34	12				

Note: $R^2 = 0.9409$, adj. $R^2 = 0.8987$ and pred.$R^2 = 0.7631$.

3.1.2. The impact of independent variables on the PDI

PDI value, the second key parameter in Design-Expert Analysis, is critical in terms of the nanoparticle formulation, stability, and controlled delivery of the SLNs to the target area. As given in Table 4, the

Table 4
ANOVA values for PDI.

Source	Sum of Squares	df	Mean Square	F Value	p-value Prob > F	
Model	0.038	5	7.613E-003	21.40	0.0004	Significant
A-ATRA	2.151E-004	1	2.151E-004	0.60	0.4623	
B-Tri	0.011	1	0.011	30.20	0.0009	
AB	8.010E-003	1	8.010E-003	22.52	0.0021	
A^2	0.017	1	0.017	46.83	0.0002	
B^2	4.326E-003	1	4.326E-003	12.16	0.0102	
Residual	2.490E-003	7	3.558E-004			
Lack of Fit	6.524E-004	3	2.175E-004	0.47	0.7175	not significant
Pure Error	1.838E-003	4	4.595E-004			
Cor Total	0.041	12				

Note: $R^2 = 0.9386$, adj. $R^2 = 0.8947$ and pred.$R^2 = 0.8148$.

PDI values were determined to be between 0.222 and 0.382. The minimum PDI value was calculated according to the following quadratic equation:

PDI: $0.25 + 5.186E\text{-}003A + 0.037B - 0.045AB + 0.049\,A^2 + 0.025\,B^2$

The variables ATRA and Tripalmitin were assigned the values of A and B, correspondingly. The regression model for PDI values was tested using ANOVA analysis, as indicated in Table 4. The significance of the model equation was established by the observation of a high F value (21.40) and a low P-value (<0.001). The insignificance of the lack of fit value for the model was determined with a p-value of 0.47. The R^2 value of the model was found to be high at 0.9386, suggesting that a significant proportion of the variability, precisely 93.86 %, could be accounted for by the model. The coefficient of determination (R^2) for the prediction model was found to be 0.8148, which was in agreement with the adj. R^2 value of 0.8987. This indicates a vigorous correlation between the predicted and observed values. The findings of the ANOVA indicated that the augmentation of Tripalmitin had a more significant impact on the PDI value ($p < 0.05$) in comparison to the rise in the quantity of ATRA ($p > 0.05$). Moreover, the 3D response surface plot depicted in Fig. 1 validates that there exists a positive correlation between the quantity of Tripalmitin and the PS increment.

3.1.3. The impact of independent variables on the EE (%)

The EE (%), the third key parameter in the Design-Expert software, was calculated using the centrifuge method as previously described [26,27]. As shown in Table 1, EE (%) of SLN was determined in different ranges from 8.6 % to 30 %. The following equation was applied to achieve the maximum EE.

EE (%): $20.14 + 7.8A + 1.07B - 2.22AB - 2.31A^2 + 3.09B^2$

The coded values for ATRA and Tripalmitin were represented by A and B, respectively. The ANOVA analysis for EE (%), utilizes the regression model (Table 5). The statistical ANOVA findings relating to EE% indicate that the model equation was considered significant, as confirmed by the high F value (27.30) and low p values (<0.001). Moreover, the absence of a significant lack of fit value ($p = 3.68$) suggests that the model was well-fitted. The statistical validity of the regression model was reinforced by an R^2 value of 0.9512, indicating that the model could account for 95.12 % of the variability in the response. The obtained values of adj.R^2 and pred.R^2, which were 0.9164 and 0.7252, respectively, exhibited consistency and suggested that the degree of variability was deemed satisfactory.

ANOVA results indicated that an increase in the amount of ATRA ($p < 0.05$) caused a significant increase in EE (%) value in comparison to the change in the amount of Tripalmitin ($p > 0.05$). Moreover, the 3D response surface graph (Fig. 1) confirmed that EE (%) was improved with the increase in the amount of ATRA used in the formulation.

3.1.4. Optimization study of ATRA-loaded SLNs

The Design-Expert software was utilized to determine the optimal formulation of ATRA-loaded PEGylated SLNs based on the outcomes of the CCD investigation. Considering the most important criteria such as the maximum EE (%), minimum PS, and PDI values, the desired limitations were established. The optimum amount of the critical substances ATRA and Tripalmitin within the formulation were found as 5.24 mg and 39.64 mg, respectively.

As given in Table 6, the predicted and experimental response data for PS of SLNs were found to be 177.28 nm and 178.2 ± 6.70 nm, respectively, where the prediction error was determined as a negligible number of 0.15 %. Accordingly, the 3D response surface graph reveals that the PS value increases as the amount of ATRA increases (Fig. 1). The increase in PS may be linked to the physicochemical properties of ATRA entrapped within tripalmitin solid core of formulation as well as surrounded by the phospholipid. Similarly, Chinsriwongkul (2009) revealed in a previous study that the average PS of ATRA-loaded SLNs increased when ATRA concentration in the formulation increased [48]. On the other hand, when the amount of tripalmitin was used in the formulation in the range of 40 ± 2 mg, there was no significant alteration in PS ($p > 0.05$) (Fig. 1). In previous studies, it has been shown that the PS of SLNs depends on the phospholipid/solid lipid (tripalmitin) ratio [25,26,46,49]. Heiati et al. (1996) revealed that an increase in the phospholipid: solid lipid molar ratio led to a decrease in PS until it reached a plateau of 0.15 %, after this point, the alteration in the ratio did not affect the PS [49]. Simultaneously, the study showed that as the phospholipid: solid lipid ratio increased, so could the likelihood of bilayer phospholipids wrapping around SLNs. Since phospholipids are energetically attracted to the oil/water phase interface, the interface must be large for phospholipids to be incorporated into the formulation, which reduces the PS to a certain extent [49]. In addition, the amount of tripalmitin used in the formulation was determined according to the ratio of phospholipid and tripalmitin (in the range of 0.14 %–0.155 %), resulting in no significant change in PS as the increase in the amount of tripalmitin ($p > 0.05$).

According to the ANOVA results of the PDI changes in the Design-Expert Program, an increase in the amount of tripalmitin led to a significant change in the PDI value, whereas increasing the amount of ATRA resulted in no significant change in the PDI values ($p > 0.05$) (Table 6, and Fig. 1). On the other hand, the predicted and experimental values for PDI were determined as 0.243 and 0.245 ± 0.01, respectively, with a negligible number of prediction error (0.8 %), which is within acceptable (should be <0.3) limits in the use of nanoparticle systems for targeting [50]. Similarly, the prediction error for the predicted and experimental responses for EE (%) was found as a negligible number of 1.4 %; where the predicted and experimental values were measured as 20.98 % and 21.2 ± 1.4 %. According to the 3D response surface graph of the EE (%), the increase in the amount of ATRA displayed a statistically significant increase in EE (%); whereas no significant change was observed in EE (%) with an increasing amount of tripalmitin ($p > 0.05$) (Table 6, and Fig. 1). It has been shown that increasing the amount of tripalmitin in which ATRA is encapsulated does not affect the EE (%), and that the encapsulation reaches saturation-plateau as a result of using the excessive amount of ATRA used in the formulation. In the previous studies, the encapsulation amount of the lipophilic compounds into tripalmitin-based-SLNs was found to be between 0.02 and 0.1 [25–27].

Overall, the results of the Design-Expert Analysis demonstrated that the experimental results were found consistent with the predicted values of the model, thereby providing the accuracy and validation of the

Table 5
ANOVA values for EE (%).

Source	Sum of Squares	df	Mean Square	F Value	p-value Prob > F	
Model	633.81	5	126.76	27.30	0.0002	Significant
A-ATRA	486.38	1	486.38	104.75	<0.0001	
B-Tri	9.15	1	9.15	1.97	0.2031	
AB	19.80	1	19.80	4.26	0.0778	
A^2	37.24	1	37.24	8.02	0.0253	
B^2	66.26	1	66.26	14.27	0.0069	
Residual	32.50	7	4.64			
Lack of Fit	23.85	3	7.95	3.68	0.1204	not significant
Pure Error	8.65	4	2.16			
Cor Total	666.32	12				

Note: $R^2 = 0.9512$ adj. $R^2 = 0.9164$ and pred.$R^2 = 0.7252$.

Table 6
Pred. and experimental results of the optimized ATRA-loaded PEGylated SLN formulations.

Responses	Pred. value	Experimental value	Prediction Error (%)
PS (nm)	177.28	178.2 ± 6.70	0.15
PDI	0.243	0.245 ± 0.01	0.8
EE (%)	20.98	21.2 ± 1.4	1.04

structural assumptions.

3.1.5. Measurement of PS, PDI, and ZP

The study involved the analysis of a minimum of five distinct PEGylated SLN formulations, which were both empty and loaded with ATRA. The characteristics of interest were evaluated for each formulation including PS, PDI, and ZP. As shown in Table 7 and Fig. 2, the average diameters of empty PEGylated SLNs were found as 146.7 ± 4.16 nm (PDI: 0.242 ± 0.005; conductivity: 0.170 ± 0.007 mS/cm) (Table 7 and Fig. 2-A), while ATRA-loaded PEGylated SLN have a larger average particle diameter: 178.2 ± 6.70 nm (PDI: 0.245 ± 0.010; conductivity: 0.170 ± 0.007 mS/cm) (Table 7 and Fig. 2-B). Comparing this value with the mean PS of empty SLNs, i.e., 178.2 ± 6.70 nm, one can suggest that the encapsulation of ATRA within SLNs led to a significant increase in the average PS of the formulation ($p \leq 0.01$) (Table 7 and Fig. 2). Moreover, the alteration in PS after the incorporation of ATRA was confirmed by the Design-Expert Program (Table 2). In addition, PS of anti-PD-L1 and anti-4-1BB – conjugated ATRA-loaded SLNs was found to be 179.6 ± 12.6 nm, and the particle concentration was 1.35e+10 particles/mL, where no observable alteration was detected in PS after the process of antibody conjugation, and the values were found to be consistent with SEM images (Fig. 3). Similar to our results, Chen et al. (2018) indicated that CD20 antibody conjugation to ATRA-loaded nanoparticles did not cause a significant alteration in the detected the sizes as a result of antibody conjugation [51].

In addition to PS and PDI, ZP influences cell uptake and therapeutic efficacy considering the stability in the physiological system and systemic toxicity of nanoparticles after administration. Although positively-charged cationic particles are thought to have higher internalization rates than their non-cationic counterparts (neutral- or negatively-charged), they display higher toxicity behavior than these systems on cancer cell lines [25,52–54]. Furthermore, positively-charged liposomes can interact with serum albumins, and the extracellular matrix, causing an early release or the aggregation of the active ingredients instead of within the target cells and thereby potentially leading to systemic toxicity [55]. Considering the risk factors beyond the efficacy, Empty and ATRA-loaded SLNs were synthesized as negatively charged carrier systems.

Accordingly, all formulations displayed a negative ZP value (Table 7 and Fig. 2): empty SLNs (−36.1 ± 2.67 mV) (Fig. 2-C) and ATRA-loaded PEGylated SLNs (−43.4 ± 7.20 mV) (Fig. 2-D). Incorporation of ATRA into SLNs shifted the ZP peak of the nanoparticle remarkably from –36.1 ± 2.67 mV to −43.4 ± 7.20 mV (Fig. 2), and empty SLNs significantly differ from ATRA-loaded SLNs with a less negative ZP value ($p \leq 0.05$), which is further linked to the negative charge of ATRA to the formulation. This result indicated that the incorporation of ATRA into SLNs caused a statistically significant change in the ZP of SLNs. Besides, the ZP value increased negatively (-charged) with the addition of cholesterol to the formulation, which is compatible with the previous study [48]. Cholesterol entering the bilayer phospholipid structure changes the membrane properties of SLN and is thought to increase the ZP value in the negative ("-") direction as a result of the interaction of the cations in the buffer solution with SLNs and decrease the surface affinity. Magarkar et al. (2014) revealed that an increase in the amount of cholesterol within the liposome formulation leads to a decrease in the binding rate of sodium ions with reducing the membrane affinity, resulting in an increase in the ZP value, accordingly [56].

Table 7
Average PS, PDI, and ZP for empty and ATRA-loaded PEGylated SLNs.

Formulations[a]	PS (nm)	PDI	ZP (mV)
Empty PEGylated SLNs	146.7 ± 4.16	0.242 ± 0.005	−36.1 ± 2.67
ATRA-loaded PEGylated SLNs	178.2 ± 6.70**	0.245 ± 0.010	−43.4 ± 7.20*

[a] At least six distinct samples were collected, with an average conductivity of 0.170 ± 0.007 mS/cm.

3.1.6. Determination of PS and concentration by NTA

The PS and concentrations of empty and ATRA-loaded PEGylated SLN were alternatively measured as particles per mL using the NTA system **(Supplementary Video).** As per the data provided by the NTA data, it can be inferred that the mean and mode of PS distributions of empty and ATRA-loaded PEGylated SLNs were determined as 177.9 ± 2.0 nm and 141.1 ± 3.5 nm (Fig. 2-A, E), and 185.8 ± 1.8 nm and 154.3 ± 7.8 nm (Fig. 2-B, F), respectively, which was compatible with the predicted and experimental particle provided by DLS measurement. In addition, particle concentrations of empty and ATRA-loaded SLNs correspond to approximately 9.58×10^{10} particles/mL (1:50 dilution from the stock empty SLN) (Fig. 2-E) and 1.39×10^{11} particles/mL (1:50 dilution from the stock ATRA-loaded SLN) (Fig. 2-F), respectively, confirming the DLS analysis that incorporation of ATRA into SLNs led to an increase in the size and concentrations. Likewise, after lyophilization, the average PS of the empty and ATRA-loaded SLNs was measured as 150.6 ± 4.32 and 177.6 ± 5.96 nm, respectively, which remained constant, and no aggregation was observed in both formulations.

On the other hand, dual antibody-conjugated-ATRA-loaded SLNs were analyzed in terms of PS and concentration using by NTA system. Accordingly, the mean of PS distribution was determined as 179.6 ± 12.6 nm, which corresponds to approximately 1.35×10^{10} particles/mL (1:50 dilution from the stock SLN), indicating that the antibody conjugation onto SLNs did not lead to a significant alteration in the PS of ATRA-loaded PEGylated SLNs further (185.8 ± 1.8 nm) ($p \geq 0.05$). On the other hand, the particle concentrations seem to decrease after antibody conjugation, as measured by NTA. According to the result obtained from the NTA analysis, the average PS was determined within the desired value for use in targeting.

3.1.7. Morphological analysis of SLNs by SEM

The SEM analysis suggested that tripalmitin composition surrounded by phospholipids successfully entraps ATRA inside its inner solid matrix. Empty and ATRA-loaded PEGylated SLNs are spherical in form and have a smooth phospholipid outer surface, allowing for stable dispersion (Fig. 3). SEM analysis demonstrated that both empty (Fig. 3-A) and ATRA-loaded PEGylated SLNs (Fig. 3-B) were spherical in morphology, and had conserved their uniform surface characteristics after encapsulation of ATRA. In parallel with the DLS and NTA analysis, SEM images confirmed that the sizes of both empty and ATRA-loaded PEGylated SLNs vary between 100 and 200 nm.

Likewise, anti-PD-L1 and anti-4-1BB-conjugated-ATRA-loaded SLNs were observed to preserve their spherical shape characteristics, and smooth surface morphology after conjugation of antibodies (Fig. 3-C). Moreover, SEM images were found consistent with the NTA data in terms of the average sizes ranging from nearly 167 to 192.2 nm.

3.1.8. Determination of ATRA content in SLN formulations

The amount of ATRA in the SLN formulation was found to be 108.6 ± 0.027 μg/mL.

3.1.9. NMR spectroscopy analysis of DSPE-PEG$_{2000}$-maleimide - modified SLNs

The ^{1}H NMR spectra of DSPE-PEG$_{2000}$-Maleimide - modified SLNs were recorded in $CDCl_3$. The main components of the synthesized system appear to have repeating units on small molecules. Thus, the main signals in the spectrum were observed in DSPE-PEG$_{2000}$-Maleimide and Tripalmitin. Accordingly, PEG's backbone methylene signals were found between 3.6 and 3.7 ppm. Vinylic protons were recorded at 6.7 ppm; whereas methylene protons of tripalmitin were recorded as multiplets between 4.1 and 4.6 ppm. Comparison of these protons with the ratio of PEG backbone protons between tripalmitin and DSPE-PEG$_{2000}$-Maleimide was calculated as 4:0.82, respectively (Fig. 4-A). Aliphatic chains

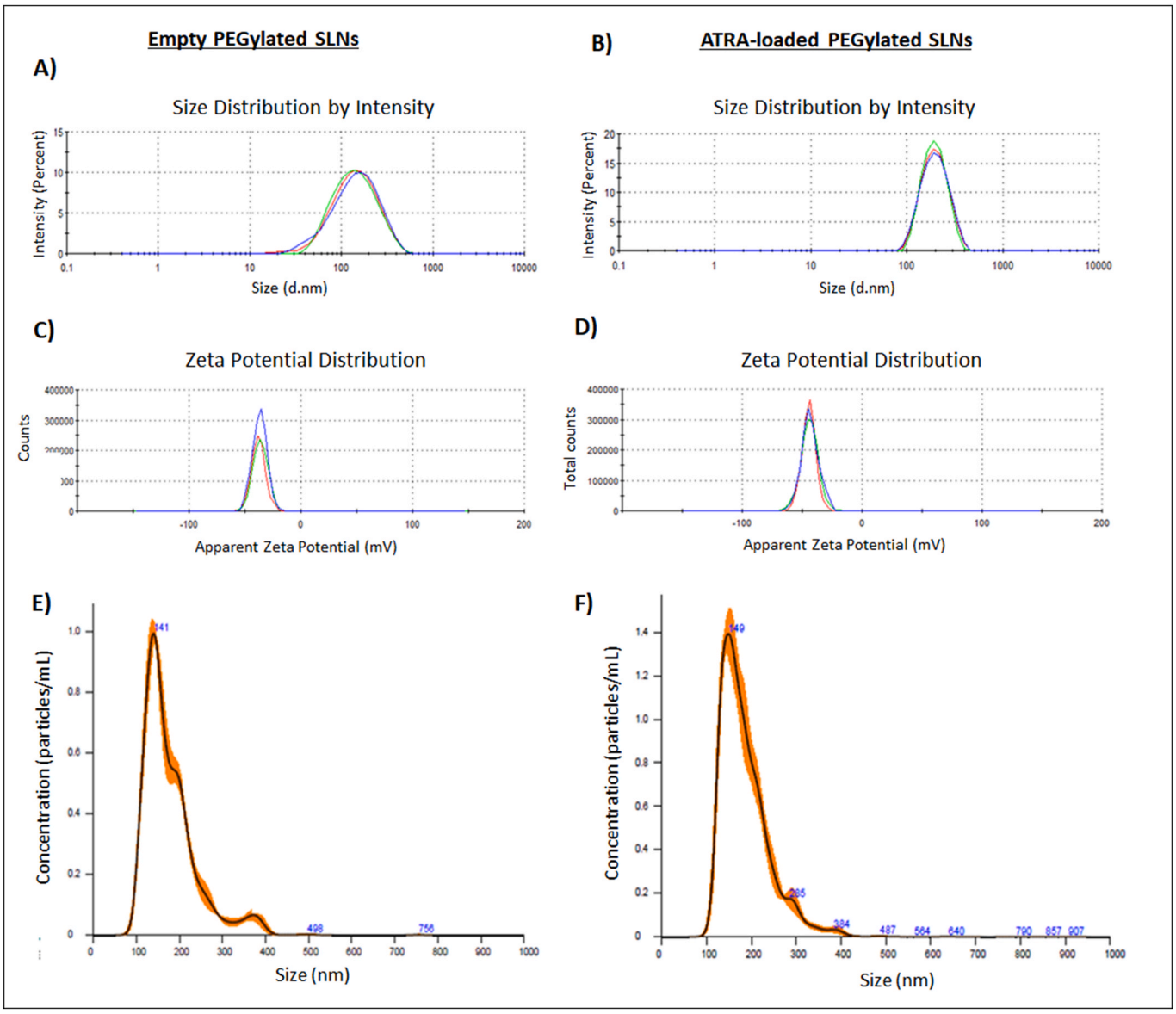

Fig. 2. The histogram analysis of **(A&B)** the PS distribution, **(C&D)** ZP, and **(E&F)** PS-concentration plot of empty and ATRA-loaded PEGylated SLNs.

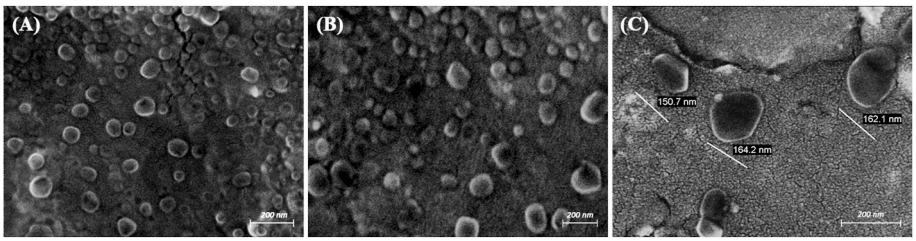

Fig. 3. Dispersity, shape, and morphology analysis of SLNs. SEM images of optimum **(A)** Empty PEGylated SLNs, **(B)** ATRA-loaded PEGylated SLNs, and **(C)** anti-PD-L1 and anti-4-1BB-conjugated-ATRA-loaded SLNs. Scale bars correspond to 200 nm.

on both structures were observed between 1.2 and 1.4 ppm, where methyl groups at the end of the aliphatic chains were found at 0.88 ppm.

3.1.10. FTIR spectroscopy analysis of DSPE-PEG$_{2000}$-maleimide - modified SLNs

The surface modifications of ATRA-loaded PEGylated SLNs were also further investigated by FTIR spectroscopy based on the functional group analysis among DSPE-PEG$_{2000}$-Maleimide and ATRA-loaded-DSPE-PEG$_{2000}$-Maleimide- modified SLNs (Fig. 4). Accordingly, the peaks of DSPE-PEG$_{2000}$-Maleimide-modified SLNs appeared at the same points (2913 cm^{-1}, 2848 cm^{-1}, 1735 cm^{-1}, 1471 cm^{-1}, 1196 cm^{-1}, 740 cm^{-1}) with DSPE-PEG$_{2000}$-Maleimide, and thus demonstrating the achievement of the modification of SLNs with DSPE-PEG$_{2000}$-Maleimide functional group (Fig. 4-B, C). Moreover, a peak appeared at 1728 cm^{-1}, indicating the carbonyl groups of DSPE-PEG$_{2000}$-Maleimide, and the peak intensity of the band showed C–O–C stretching of C–O at 1243

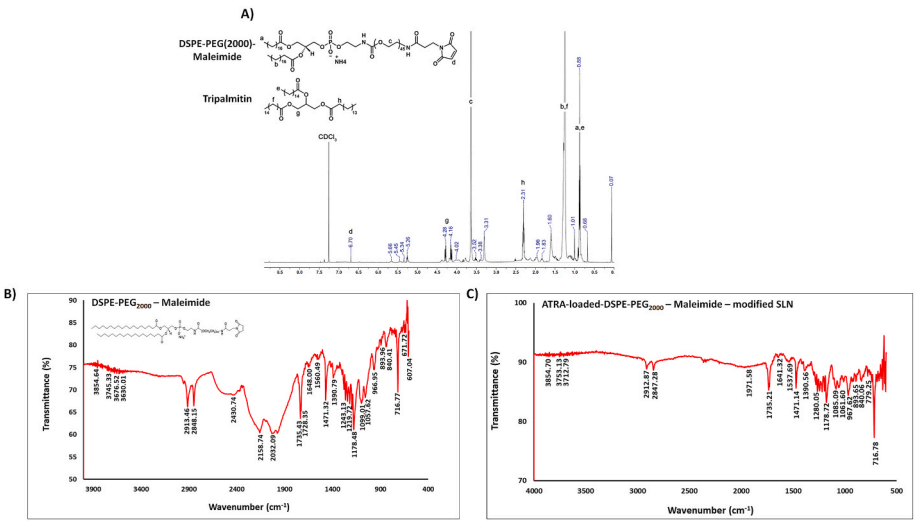

Fig. 4. ^{1}H NMR spectra of DSPE-PEG$_{2000}$-Maleimide modified SLNs **(A),** and FTIR spectra of **(B)** DSPE-PEG$_{2000}$-Maleimide, and **(C)** ATRA-loaded- DSPE-PEG$_{2000}$-Maleimide – modified SLN.

cm^{-1} and the repeated unit of PEG (-OCH_2CH_2) at 1109 cm^{-1} (Fig. 4-B, C). Also, the specific peaks of DSPE-PEG$_{2000}$-Maleimide-modified SLNs were observed at 1641 and 1648 cm^{-1}, corresponding to C=O stretching (Fig. 4-C).

3.1.11. DSC analysis of SLN formulations

Empty and ATRA-loaded PEGylated SLN formulations were evaluated in terms of melting and crystallization behavior by DSC analysis. According to DSC thermograms (Fig. 5), the melting process for empty and ATRA-loaded SLNs was measured to maximum peaks at 64.98 and 64.25 °C, respectively, indicating that no crystal formation was observed in the SLN formulations (Fig. 5-A, B).

3.1.12. Determination of the antibody conjugation

The bond structure of DSPE-PEG-maleimide, which is added to the formulation for the surface modification, is thought to be disrupted by the use of ultrasonication, during the SLN synthesis using the lipid film hydration method [37,57]. The functionalization of nanoparticles is hindered by the hydrolysis of maleimides, resulting in an increase in negative charge due to the formation of maleic acid as a hydrolysis product [37]. Moreover, hydrolysis leads to an alteration in the surface functionalization as a result of the formation of free carboxyl groups [37, 58]. To achieve DSPE-PEG-Maleimide modification, two common preparation methods were demonstrated previously for the surface functionalization [38,59], which can be described as pre-insertion of DSPE-PEG2000-Mal (during) or post-insertion method (after SLN preparation process). Oswald and colleagues (2016) investigated the modification process of liposomes with the DSPE-PEG-maleimide group by pre-insertion and post-insertion methods [37]. The study revealed that the liposomes prepared through pre-insertion carried 63 % maleimide group and decreased to 32 % by the purification process; whereas 76 % of the maleimide group was determined on the liposome surface using the post-insertion method [37]. In our study, DSPE-PEG-Maleimide modification was achieved by the post-insertion method, where SLNs were mixed with DSPE-PEG-Maleimide overnight at a constant rate after sonication and centrifugation, the final step of production, as described in the previous studies [37,38,59,60].

Accordingly, mAbs were covalently bound in their thiolated form to sulfhydryl reactive groups that were introduced by a DSPE-PEG2000-maleimide onto the surface of SLNs. Characterization of thiolated monoclonal antibodies, as well as antibody conjugated-SLNs, are crucial for the determination of the quality of the optimized SLNs. Therefore, the following characterization studies were performed for anti-PD-L1 and anti-4-1BB-conjugated- ATRA-loaded-SLNs.

3.1.13. Quantification of antibody thiolation by Ellman's reagent

The concentrations of sulfhydryl groups per thiolated-anti-IgG (1 mg/mL), thiolated-anti-4-1BB (100 μg/mL) and thiolated-anti-PD-L1 (100 μg/mL) were found to be 7.71×10^{-4} M, 0.75×10^{-4} M and 0.74×10^{-4} M, respectively, indicating that the amount of antibodies involved in the reaction and their thiolation rates were correlated with each other.

3.1.14. SDS-PAGE analysis of dual antibody-conjugated SLNs

The presence of antibody-conjugated to the SLN and the antibody integrity was determined by SDS-PAGE electrophoresis. As expected, empty and ATRA-loaded PEGylated SLN without antibodies produced no protein fragments (Fig. 6-A, B, and C); whereas 100 and 1000 μg/mL free anti-IgG antibodies produced a band at approximately 85 kDa with different band intensities according to the concentration of the antibody added to the conjugation (Fig. 6-A). Likewise, the band thickness of SLN conjugated with 100 and 1000 μg/mL anti-IgG or anti-4-1BB antibodies increased depending on the amount of the conjugated antibody (Fig. 6-A, B). On the other hand, free anti-4-1BB and anti-PD-L1 antibodies produced two distinct bands at 33 kDa and 70 kDa, which corresponds to the light and heavy chains of the antibody, respectively, indicating that

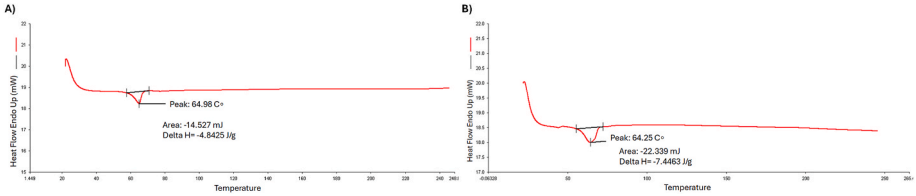

Fig. 5. DSC thermograms of **(A)** Empty, and **(B)** ATRA-loaded PEGylated SLN formulations.

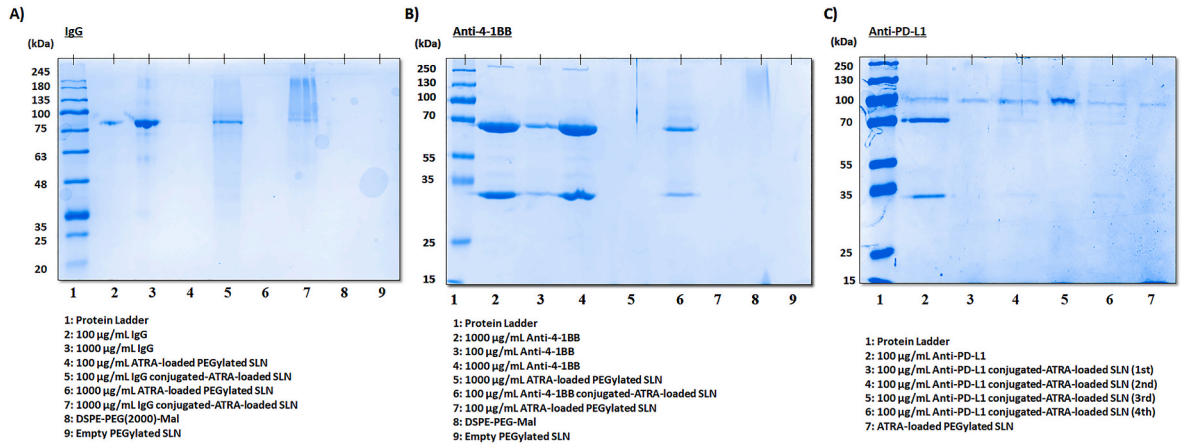

Fig. 6. SDS-PAGE electrophoresis images of mAbs unconjugated or conjugated to SLNs. The gel images of **(A)** anti-IgG antibody conjugation to SLN: (1) Protein ladder, (2) 100 µg/mL thiolated IgG, (3) 1000 µg/mL thiolated IgG, (4) 100 µg/mL ATRA-loaded PEGylated SLN, (5) 100 µg/mL IgG conjugated-ATRA-loaded-SLN, (6) 1000 µg/mL ATRA-loaded PEGylated SLN, (7) 1000 µg/mL IgG conjugated-ATRA-loaded-SLN, (8) DSPE-PEG_{2000}-Maleimide, and (9) Empty PEGylated SLN; **(B)** anti-4-1BB antibody conjugation to SLN: (1) Protein ladder, (2) 1000 µg/mL thiolated anti-4-1BB, (3) 100 µg/mL thiolated anti-4-1BB, (4) 1000 µg/mL thiolated anti-4-1BB (2nd replicate), (5) 1000 µg/mL ATRA-loaded PEGylated SLN, (6) 100 µg/mL anti-4-1BB conjugated-ATRA-loaded-SLN, (7) 100 µg/mL ATRA-loaded PEGylated SLN, (8) DSPE-PEG_{2000}-Maleimide, and (9) Empty PEGylated SLN; **(C)** anti-PD-L1 antibody conjugation to SLN: (1) Protein ladder, (2) 100 µg/mL thiolated anti-PD-L1, (3) 100 µg/mL anti-PD-L1 conjugated ATRA-loaded SLN (1st replicate), (4) 100 µg/mL anti-PD-L1 conjugated ATRA-loaded SLN (2nd replicate), (5) 100 µg/mL anti-PD-L1 conjugated ATRA-loaded SLN (3rd replicate), (6) 100 µg/mL anti-PD-L1 conjugated ATRA-loaded SLN (4th replicate), and (7) 100 µg/mL ATRA-loaded PEGylated SLN.

the protein did not undergo degradation (Fig. 6-B, C). Similarly, the characteristic two-band of both anti-4-1BB and anti-PD-L1 antibodies appeared at the same molecular weight with dual antibody – conjugated-ATRA-loaded SLNs (Fig. 6-A). The SDS-PAGE analysis demonstrates that antibodies were successfully conjugated to the DSPE-PEG_{2000}-Maleimide- modified SLNs.

Likewise, Dinauer et al. (2005) applied SDS-PAGE method for antibody detection in antibody-conjugated nanoparticles. Accordingly, proteins remaining in the supernatant and conjugated to SLNs were run on the gel and, their bands were then visualized to determine the presence of the proteins in the SLN formulations [61]. Furthermore, Steinhauser and colleagues (2006) reported that thiolated trastuzumab completely bound to nanoparticles modified with PEG-Maleimide [43], indicating the reliability and compatibility of the binding efficacy with using the modified procedure.

3.1.15. Determination of the amount of antibodies conjugated to SLNs by Bradford Protein Assay

The amount of anti-IgG, anti-4-1BB, and anti-PD-L1 mAbs conjugated to SLNs was determined by Bradford Protein Assay and the % binding efficiency of anti-IgG antibody used for optimization studies was calculated according to the polynomial plot. The binding efficiencies (%) of 100 µg/mL and 1000 µg/mL thiolated- anti-IgG antibodies to SLNs were calculated as 90.41 ± 0.12 % and 96.66 ± 0.11 %, respectively, indicating that the binding efficiency increased depending on the amount of antibodies used in the conjugation. Moreover, thiolated antibodies were successfully conjugated to DSPE-PEG_{2000}-Maleimide – modified SLNs, with the binding efficiency of 85.59 ± 7.33 % and 90.02 ± 5.4 %, respectively, and there was no statistically significant difference observed in the quantity of antibodies conjugated to the SLNs.

3.1.16. Determination of the amount of antibodies per SLNs by flow cytometry analysis

The amounts of FTIC-labeled-anti-PD-L1 (green) and PE-labeled-anti-4-1BB (red) antibodies per nanoparticle were measured by flow cytometry. The histogram analysis indicated that anti-4-1BB and anti-PD-L1 antibodies were conjugated to SLNs at a 1:1 (v/v) ratio (Fig. 7). The amount (%) of antibodies per nanoparticle were measured as 99.35 ± 1.21 % and 99.03 ± 1.84 % respectively, confirming that no significant difference was found among the percentage of antibody conjugated to SLN (Fig. 7-A, B).

Overall, the results obtained in the characterization of SLN formulations revealed that the encapsulation of ATRA into SLNs led to an increase in the PS and ZP of the formulation. The synthesis of SLNs conjugated with dual mAbs was obtained with an average diameter of 179.6 ± 12.6 nm, displaying no significant change in the PS of SLNs after conjugation. On the other hand, the binding efficiency of

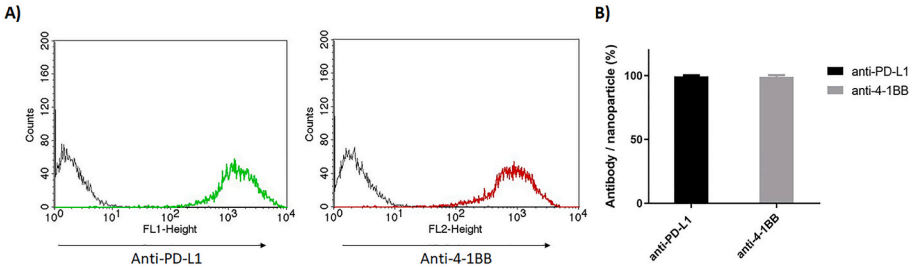

Fig. 7. Percentage of FTIC-labeled-anti-PD-L1 (green) and PE-labeled-anti-4-1BB (red) antibodies per nanoparticles (for 24 h), as determined by flow cytometry. **(A)** Histogram plot representation of fluorescently labeled anti-PD-L1 and anti-4-1BB at FL1 and FL2 filters with regard to the excitation (PE at 566 nm; FITC at 491 nm) and emission (for PE at 574 nm; FITC at 516 nm), respectively, and **(B)** Graphical demonstration. Data represents mean ($n \geq 3$) ± SD. No significant differences among antibodies per each particle, as determined by unpaired *t*-test.

antibodies to SLNs varied as ranging from 85.59 to 90.02 %, revealing the antibody conjugation by SDS-PAGE, Bradford Protein Assay, and flow cytometry analysis.

3.1.17. *In vitro* ATRA release from SLN formulations

The in vitro drug release profile was determined by the dialysis membrane diffusion method. Accordingly, the drug release profile of all SLN formulations displayed a biphasic release of ATRA from nanoparticles with the Higuchi model (r^2:0.9825 for ATRA-loaded SLNs; r^2:0.9874 for antibody-conjugated SLN), considering the highest value of the correlation coefficients (r^2) (**Supplementary Table 1**). Upon the end of the drug's release process, the antibody conjugation did not lead to a change in drug release statistically, of which approximately 85 ± 2.86 % and 76 ± 4.40 % of ATRA were cumulatively released from ATRA-loaded PEGylated SLNs and antibody-conjugated-ATRA-loaded SLNs within the first 24 h, respectively (Fig. 8).

3.1.18. Stability studies of SLN formulations

The optimum empty and ATRA-loaded PEGylated SLNs were stored at 4 ± 1 °C in the refrigerator, 25 ± 2 °C (60 % RH), and 40 ± 2 °C (75 % RH) for 9 months (at predetermined time intervals - days 0, 15, 30, 45, 60, 150, 210 and 270) in the stability cabinets, and examined for their size, ZP, and pH. In addition, stability studies of anti-PD-L1-anti-4-1BB-conjugated-ATRA loaded SLN formulations were performed under the same conditions for 2 months.

As shown in Fig. 2, no significant change in both the PS distributions and ZP of empty SLNs was observed at 4 °C and 25 ± 2 °C, 60 % RH for 9 months ($p \geq 0.05$), demonstrating the structural integrity was preserved in empty SLN formulations. However, an increase in temperature up to 40 ± 2 °C, 75 % RH resulted in a significant decrease in both PS (i.e., 9 % decrease) ($p \leq 0.05$), and ZP (i.e., 20 % decrease) ($p \leq 0.001$) of empty SLNs (Table 8). On the other hand, ATRA-loaded SLNs stored at 4 °C and 25 °C, 60 % RH did not show any significant alterations in PS and ZP values ($p \geq 0.05$), which could be related to their solid lipid content and multilamellar structure [26]. The previous study has shown that tripalmitin-based nanoparticles can be stored at 4 °C for at least 1 month [26], while amphotericin B-loaded emulsomes can remain stable for at least 3 months [62]. Ucisik et al. (2013) revealed that tripalmitin-based emulsomes conserved their PS and ZP even when stored in a refrigerator at 4 °C for an extended period [26]. Moreover, the previous study revealed that formulations preserved their particle characteristics even after a long time storage of −20 °C when lyophilized with cryoprotectants such as trehalose [49].

In addition, the ZP of ATRA-loaded SLNs did not change significantly at 40 ± 2 °C, 75 % RH for 9 months. This could be linked to the incorporation of ATRA into SLNs, which increases the ZP value associated with an acidic property of ATRA (Table 8). On the other hand, the PS distributions of anti-PD-L1 and anti-4-1BB-conjugated-ATRA-loaded SLNs showed statistically significant changes with an increase of 7 % (i.e., 190.5 ± 7.63 nm) and 11 % (i.e., 199.4 ± 5.63 nm), respectively, at 4 °C and 25 °C, 60 % relative humidity for 2 months. No statistically significant difference was observed in the pH values of all SLN formulations at 4 °C, 25 ± 2 °C, 60 % RH, and 40 ± 2 °C, 75 % RH (Table 8).

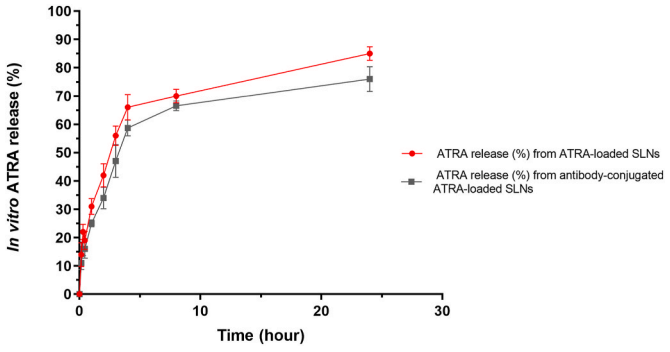

Fig. 8. *In vitro* drug release (%) plots of ATRA-loaded SLN and antibody-conjugated SLN formulations at 0–24 h time interval.

Table 8
The values of the stability parameters for optimized empty and ATRA-loaded SLN formulations in various stability conditions.

Stability parameters[a]	Day 0	Day 270 (9 months)		
		4 °C	25 ± 2 °C (60 % RH)	40 ± 2 °C (75 % RH)
PS (nm)				
Empty PEGylated SLN	142 ± 1.43	141 ± 3.24	149 ± 3.7	129 ± 3.9[a]
ATRA-loaded PEGylated SLN	178.6 ± 5.27	172 ± 2.89	181 ± 2.5	156 ± 1.5[a]
ZP (mV)				
Empty PEGylated SLN	−36.1 ± 2.67	−34.2 ± 3.68	−31.8 ± 5.24	−28.8 ± 1.24***
ATRA-loaded PEGylated SLN	−48.5 ± 6.29	−49.2 ± 5.35	−40.5 ± 6.17	−46.3 ± 2.19
pH				
Empty PEGylated SLN	7.4	7.32 ± 0.01	7.32 ± 0.02	7.22 ± 0.01
ATRA-loaded PEGylated SLN	7.4	7.4 ± 0.01	7.36 ± 0.01	7.29 ± 0.01

[a] Standard deviations of values correspond to the average standard deviation of all measurements, where n ≥ 3 ± SD. Statistical significance was determined using ordinary one-way ANOVA, with Tukey's multiple-comparison test (ns: not significant, (*) P ≤ 0.05, (**) P ≤ 0.01, (***) P ≤ 0.001, and (****) P ≤ 0.0001).

4. Conclusion

Anti-PD-L1 checkpoint inhibitors and 4-1BB co-stimulatory molecules have recently come forward with anti-cancer therapy beyond the standard, conventional chemotherapeutic agents. However, the exposed lower level activity on cancer cells compared to being given alone, and higher toxicity with the increased dosage of the drugs, especially in combination. Moreover, synergistic activity was reported when co-administered with ATRA, an active chemotherapeutic agent, necessitating the combinational approach using using solid-based lipid nanoparticles. Otherwise, due to the low toxicity profile and lower bioavailability of ATRA, the medical use might remain limited rather than encapsulated form within SLNs. The presented study introduced anti-PD-L1 and anti-4-1BB-conjugated ATRA-loaded SLNs as promising targeted drug delivery systems to address these limitations. In this way, Kosmides et al. have set the framework for the development of the anti-PD-L1 and anti-4-1BB- conjugated iron-dextran particles to deliver tumor cells, thus resulting in the inhibition of checkpoint PD-L1 signal, and activate T cells through the 4-1BB co-stimulation for the delay on tumor survival [19]. Similarly, Chen et al. designed the poly (lactic acid-co-glycolic acid)-block-poly(ethylene glycol) (PLGA-PEG) nanocarriers to conjugate ATRA, and PD-L1 antibody was incorporated to enable targeted therapy for oral squamous cell carcinoma (OSCC) and oral dysplasia. The ATRA–PLGA-PEG–PD-L1 nanoparticles had superior tumor-targeting ability compared to the control group, as evidenced by whole-animal fluorescence imaging, and further multicolor immunohistochemistry analysis demonstrated successful modulation of protein expression following nanoparticle therapy [63]. In another study, ATRA was used to improve the therapeutic effect of anti-PD-L1 treatment in cervical cancer by suppressing the function of myeloid-derived suppressive cells. Based on the study, the co-administration of ATRA and anti-PD-L1 antibody resulted in a profound inhibition of U14 tumor growth and led to an increased percentage of $CD62L^{-}CD8^{+}$ T cells, $CD62L^{-}CD4^{+}$ T cells, $CD107a^{+}CD8^{+}$ T cells, as well as elevated levels of IFN-γ and TNF-α within the tumors [10].

Considering the advantage of combination therapy of anti-PD-L1 and

ATRA or anti-4-1BB in cancer treatments, herein, we focus on the experimental Design-Expert Analysis used for the optimization study of nanoparticles, in which the characterization studies were well-designed based on the antibody conjugation strategies in detail. In addition, the DSPE-PEG-maleimide PEGylation strategy was used in the surface modification of anti-PD-L1 and anti-1BB conjugation to nanoparticles by pre- and post-insertion methods, which were not prioritized in previous studies. The results demonstrate that the Design Expert Analysis indicated the accuracy of the method associated with the correlation of the predicted and adjusted values belonging to the critical parameters (i.e., PS, PDI, and EE (%). The overall characterizations of the initial empty form to antibody-conjugated SLNs were studied through analysis of physicochemical features (i.e., PS, PDI, and ZP), morphology taken from SEM images, various protein analyses including SDS-PAGE, Bradford Assay, and flow cytometry analysis, *in vitro* drug release, and the stability analysis to further provide which the fate of the nanoparticles interact with its storage condition. Besides, the PEGylated SLNs were analyzed in terms of the presence of a functional DSPE-PEG Maleimide group for the determination of surface modification, and crystalization properties, using FTIR, NMR Analysis, and DSC. Observed morphological properties such as spherical shape, and uniform dispersion were obvious signs of the presence of SLNs. It is the first study that emphasizes to use of DTT (reducing agent) together with Traut's Reagent for the antibody thiolation study, indicating the higher thiolation rate and binding efficacy considering the characterization studies.

Based on these results, the proposed experimental design illustrates an accurate and relatively well-designed for for the development of ATRA-loaded anti-PD-L1 and anti-4-1BB-conjugated lipid-based targeted drug delivery. The use of Design Expert Analysis and PEG-based functionalization allows precisely synthesized SLNs in line with the intrinsic characteristics of each compound, and emphasizes the system's potential for further *in vitro*, *in vivo,* and clinical studies investigations. It is important to note that the current investigation represents the first report revealing SLNs as the nanocarrier mechanism that attains anti-PD-L1 and anti-4-1BB conjugation in conjunction with ATRA integration.

Funding

The financial support was provided by Yeditepe University, Turkiye. The authors declare that no funds, grants, or other support were received during the preparation of this manuscript.

Disclosure statement

No potential competing interest was reported by the authors.

Ethical standards

No animal or human studies were carried out by the authors of this article.

Statements & declarations

Zeynep Islek, Ali Asram Sagiroglu, Mehmet Hikmet Ucisik, Oguz Kaan Kirbas, Erhan Demirel, Aysu Yurdasiper, Fikrettin Sahin, and Kevser Ozgen Ozer declare that they have no conflict of interest. The authors declare that no funds, grants, or other support were received during the preparation of this manuscript. No animal or human studies were carried out by the authors for this article.

CRediT authorship contribution statement

Zeynep Islek: Writing – review & editing, Writing – original draft, Visualization, Validation, Software, Methodology, Investigation, Formal analysis, Data curation, Conceptualization. **Ali Asram Sagiroglu:** Writing – review & editing, Writing – original draft, Methodology, Investigation, Formal analysis. **Mehmet Hikmet Ucisik:** Writing – review & editing, Investigation, Formal analysis, Conceptualization. **Oguz Kaan Kirbas:** Writing – review & editing, Methodology, Investigation. **Erhan Demirel:** Writing – review & editing, Methodology, Investigation, Formal analysis. **Aysu Yurdasiper:** Writing – review & editing, Methodology, Investigation. **Fikrettin Sahin:** Writing – review & editing, Resources, Methodology. **Ozgen Ozer:** Writing – review & editing, Writing – original draft, Validation, Supervision, Methodology, Investigation, Conceptualization.

Declaration of competing interest

The authors declare that they have no known competing financial interests or personal relationships that could have appeared to influence the work reported in this paper.

Data availability

The authors do not have permission to share data.

Acknowledgment

The authors would like to thank Murat Ozpolat for their assistance with flow cytometry, and Pınar Akkus for her support in FTIR studies.

Appendix A. Supplementary data

Supplementary data to this article can be found online at https://doi.org/10.1016/j.jddst.2024.105995.

Abbreviations

Adj	Adjusted
Anti-IgG	Anti-Immunoglobulin G
Anti-PD-L1	Anti-programmed death-ligand 1
ATRA	All-trans retinoic acid
CCD	Central Composite Design
3D	Three-dimensional
DDS	Drug Delivery System
DSPE-PEG(2000) Amine	1,2-distearoyl-sn-glycero-3-phosphoethanolamine-N-[amino(polyethylene glycol)-2000]
DSPE-PEG2000 maleimide	1,2-distearoyl-sn-glycero-3-phosphoethanolamine-N [maleimide (polyethylene glycol)-2000]
EE	Encapsulation Efficiency
FITC	Fluorescent Isothiocyanate
FTIR	Fourier-transform Infrared Spectroscopy
mAb	monoclonal antibody
MPS	Mononuclear Phagocyte System
MDSC	Myeloid-derived Suppressive Cell
NMR	Nuclear Magnetic Resonance
NTA	Nanoparticle Tracking Analysis
PDI	Polydispersity index
PE	Phytoerythrin
PEG	Polyethylene glycol
PS	Particle size
PLGA	Poly(lactide-co-glycolide acid)
PLGA–PEG	Poly(lactide-co-glycolide acid)-poly(ethylene glycol)
Pred	Predicted
RP-HPLC	Reversed-phase high-pressure liquid chromatography
SDS-PAGE	Sodium Dodecyl Sulfate-Polyacrylamide Gel Electrophoresis
SLNs	Solid lipid nanoparticles
Tri	Tripalmitin
Two-way ANOVA	Two-way Analysis of Variance

ZP Zeta potential

References

[1] Y. Shindo, K. Yoshimura, A. Kuramasu, Y. Watanabe, H. Ito, T. Kondo, A. Oga, H. Ito, S. Yoshino, S. Hazama, K. Tamada, H. Yagita, M. Oka, Combination immunotherapy with 4-1BB activation and PD-1 blockade enhances antitumor efficacy in a mouse model of subcutaneous tumor, Anticancer Res. 35 (1) (2015) 129–136.

[2] A.W. Tolcher, M. Sznol, S. Hu-Lieskovan, K.P. Papadopoulos, A. Patnaik, D. W. Rasco, D. Di Gravio, B. Huang, D. Gambhire, Y. Chen, A.D. Thall, N. Pathan, E. V. Schmidt, L.Q.M. Chow, Phase Ib study of utomilumab (PF-05082566), a 4-1BB/CD137 agonist, in combination with pembrolizumab (MK-3475) in patients with advanced solid tumors, Clin. Cancer Res. (2017), https://doi.org/10.1158/1078-0432.CCR-17-1243.

[3] T. Bartkowiak, M.A. Curran, 4-1BB agonists: multi-potent potentiators of tumor immunity, Front. Oncol. (2015), https://doi.org/10.3389/fonc.2015.00117.

[4] A. Mukhopadhaya, Nobel prize in physiology or medicine – 2018, Resonance (2018), https://doi.org/10.1007/s12045-018-0746-4.

[5] E.I. Buchbinder, A. Desai, CTLA-4 and PD-1 pathways similarities, differences, and implications of their inhibition, Am. J. Clin. Oncol. Cancer Clin. Trials (2016), https://doi.org/10.1097/COC.0000000000000239.

[6] S.C. Wei, N.-A.A.S. Anang, R. Sharma, M.C. Andrews, A. Reuben, J.H. Levine, A. P. Cogdill, J.J. Mancuso, J.A. Wargo, D. Pe'er, J.P. Allison, Combination anti–CTLA-4 plus anti–PD-1 checkpoint blockade utilizes cellular mechanisms partially distinct from monotherapies, Proc. Natl. Acad. Sci. U. S. A 116 (45) (2019) 22699–22709, https://doi.org/10.1073/pnas.1821218116. Epub 2019 Oct 21.

[7] E. Perez-Ruiz, I. Etxeberria, M.E. Rodriguez-Ruiz, I. Melero, Anti-CD137 and PD-1/PD-L1 antibodies en route toward clinical synergy, Clin. Cancer Res. (2017), https://doi.org/10.1158/1078-0432.CCR-17-1799.

[8] S. Chen, L.F. Lee, T.S. Fisher, B. Jessen, M. Elliott, W. Evering, K. Logronio, G. H. Tu, K. Tsaparikos, X. Li, H. Wang, C. Ying, M. Xiong, T. Van Arsdale, J.C. Lin, Combination of 4-1BB agonist and PD-1 antagonist promotes antitumor effector/memory CD8 T cells in a Poorly Immunogenic Tumor Model, Cancer Immunol. Res. (2015), https://doi.org/10.1158/2326-6066.CIR-14-0118.

[9] A. Muik, I. Altintas, F. Gieseke, K.B. Schoedel, S.M. Burm, A. Toker, T.W. Salcedo, D. Verzijl, D. Eisel, C. Grunwitz, L.M. Kranz, M. Vormehr, D.P.E. Satijn, M. Diken, S. Kreiter, K. Sasser, T. Ahmadi, Ö. Türeci, E.C.W. Breij, M. Jure-Kunkel, U. Sahin, An Fc-inert PD-L1×4-1BB bispecific antibody mediates potent anti-tumor immunity in mice by combining checkpoint inhibition and conditional 4-1BB co-stimulation, OncoImmunology (2022), https://doi.org/10.1080/2162402X.2022.2030135.

[10] M.Y., C.Z. Yun Liang, Wenshan Wang, Xiaojun Zhu, Inhibition of myeloid-derived suppressive cell function with all-trans retinoic acid enhanced anti-PD-L1 efficacy in cervical cancer, Sci. Rep. 12 (2022).

[11] J.J.L. Daniel, J. Olson, Myeloid maturity: ATRA to enhance anti-PD-1? Clin. Cancer Res. 22 (2023).

[12] J. Zhou, Z, H. Wang, J. Li, X. Jiang, Z. Li, Shen, Recent progress, perspectives, and issues of engineered PD-L1 regulation nano-system to better cure tumor: a review, Int. J. Biol. Macromol. 254 (2024) 127911, https://doi.org/10.1016/j.ijbiomac.2023.127911.

[13] J. hao Li, L. jia Huang, H. ling Zhou, Y. ming Shan, F. min Chen, V.P. Lehto, W. jun Xu, L. qiang Luo, H. jun Yu, Engineered nanomedicines block the PD-1/PD-L1 axis for potentiated cancer immunotherapy, Acta Pharmacol. Sin. (2022), https://doi.org/10.1038/s41401-022-00910-w.

[14] P. Song, X. Zhao, S. Xiao, Application prospect of peptide-modified nano targeting drug delivery system combined with PD-1/PD-L1 based immune checkpoint blockade in glioblastoma, Int. J. Pharm. (2020), https://doi.org/10.1016/j.ijpharm.2020.119865.

[15] R.Y., Y.W. Weinan Li, Yuhan Fu, Jialin Sun, Hexin Gong, Construction and in vitro evaluation of pH-sensitive nanoparticles to reverse drug resistance of breast cancer stem cells, Discov. Oncol. 15 (2024) 21, https://doi.org/10.1007/s12672-024-00873-w.

[16] S. Suzuki, S. Kawakami, N. Chansri, F. Yamashita, M. Hashida, Inhibition of pulmonary metastasis in mice by all-trans retinoic acid incorporated in cationic liposomes, J. Contr. Release (2006), https://doi.org/10.1016/j.jconrel.2006.08.025.

[17] X.J. Chen, X.Q. Zhang, M.X. Tang, Q. Liu, G. Zhou, Anti-PD-L1-modified and ATRA-loaded nanoparticles for immuno-treatment of oral dysplasia and oral squamous cell carcinoma, Nanomedicine (2020), https://doi.org/10.2217/nnm-2019-0397.

[18] Z. Shen, A. Fisher, W.K. Liu, Y. Li, PEGylated "stealth" nanoparticles and liposomes, in: Eng. Biomater. Drug Deliv. Syst. Beyond Polyethyl. Glycol, 2018, https://doi.org/10.1016/B978-0-08-101750-0.00001-5.

[19] A.K. Kosmides, J.W. Sidhom, A. Fraser, C.A. Bessell, J.P. Schneck, Dual targeting nanoparticle stimulates the immune system to inhibit tumor growth, ACS Nano 11 (2017) 5417–5429, https://doi.org/10.1021/acsnano.6b08152.

[20] Y. Moon, M.K. Shim, J. Choi, S. Yang, J. Kim, W.S. Yun, H. Cho, J.Y. Park, Y. Kim, J.K. Seong, K. Kim, Anti-PD-L1 peptide-conjugated prodrug nanoparticles for targeted cancer immunotherapy combining PD-L1 blockade with immunogenic cell death, Theranostics (2022), https://doi.org/10.7150/thno.69119.

[21] R.H. Fang, W. Gao, L. Zhang, Targeting drugs to tumours using cell membrane-coated nanoparticles, Nat. Rev. Clin. Oncol. (2023), https://doi.org/10.1038/s41571-022-00699-x.

[22] A.C. Anselmo, S. Mitragotri, Nanoparticles in the clinic: an update, Bioeng. Transl. Med. (2019), https://doi.org/10.1002/btm2.10143.

[23] A.C. Anselmo, S. Mitragotri, Nanoparticles in the clinic: an update post COVID-19 vaccines, Bioeng. Transl. Med. (2021), https://doi.org/10.1002/btm2.10246.

[24] J. Huang, K. Xiao, Nanoparticles-based strategies to improve the delivery of therapeutic small interfering RNA in precision oncology, Pharmaceutics (2022), https://doi.org/10.3390/pharmaceutics14081586.

[25] M.H. Ucisik, S. Küpcü, M. Debreczeny, B. Schuster, U.B. Sleytr, S-layer coated emulsomes as potential nanocarriers, Small 9 (2013) 2895–2904, https://doi.org/10.1002/smll.201203116.

[26] M.H. Ucisik, S. Küpcü, B. Schuster, U.B. Sleytr, Characterization of CurcuEmulsomes: nanoformulation for enhanced solubility and delivery of curcumin, J. Nanobiotechnol. (2013), https://doi.org/10.1186/1477-3155-11-37.

[27] Z.B. Bolat, Z. Islek, B.N. Demir, E.N. Yilmaz, F. Sahin, M.H. Ucisik, Curcumin- and piperine-loaded emulsomes as combinational treatment approach enhance the anticancer activity of curcumin on HCT116 colorectal cancer model, Front. Bioeng. Biotechnol. (2020), https://doi.org/10.3389/fbioe.2020.00050.

[28] Z. Islek, M.H. Ucisik, E. Keskin, B.O. Sucu, A.G. Gomes-Alves, A.M. Tomás, M. Guzel, F. Sahin, Antileishmanial activity of BNIPDaoct- and BNIPDanon-loaded emulsomes on leishmania infantum parasites, Front. Nanotechnol. (2022), https://doi.org/10.3389/fnano.2021.773741.

[29] N.A. Alhakamy, S.M. Badr-Eldin, O.A.A. Ahmed, H.Z. Asfour, H.M. Aldawsari, M. M. Algandaby, B.G. Eid, A.B. Abdel-Naim, Z.A. Awan, A.F. Alghaith, A.L. Alaofi, A. I. Mohamed, S.Z. Okbazghi, M.W. Al-Rabia, U.A. Fahmy, Piceatannol-loaded emulsomes exhibit enhanced cytostatic and apoptotic activities in colon cancer cells, Antioxidants (2020), https://doi.org/10.3390/antiox9050419.

[30] T. Li, S. Takeoka, A novel application of maleimide for advanced drug delivery: in vitro and in vivo evaluation of maleimide-modified pH-sensitive liposomes, Int. J. Nanomed. (2013), https://doi.org/10.2147/IJN.S47749.

[31] K. Renault, J.W. Fredy, P.Y. Renard, C. Sabot, Covalent modification of biomolecules through maleimide-based labeling strategies, Bioconjugate Chem. (2018), https://doi.org/10.1021/acs.bioconjchem.8b00252.

[32] M. Izci, C. Maksoudian, B.B. Manshian, S.J. Soenen, The use of alternative strategies for enhanced nanoparticle delivery to solid tumors, Chem. Rev. (2021), https://doi.org/10.1021/acs.chemrev.0c00779.

[33] Y. Xiao, J. Chen, H. Zhou, X. Zeng, Z. Ruan, Z. Pu, X. Jiang, A. Matsui, L. Zhu, Z. Amoozgar, D.S. Chen, X. Han, D.G. Duda, J. Shi, Combining p53 mRNA nanotherapy with immune checkpoint blockade reprograms the immune microenvironment for effective cancer therapy, Nat. Commun. (2022), https://doi.org/10.1038/s41467-022-28279-8.

[34] S. Gürcan, N. Tsapis, F. Reynaud, S. Denis, J. Vergnaud, Ö. Özer, E. Fattal, Combining dexamethasone and TNF-α siRNA within the same nanoparticles to enhance anti-inflammatory effect, Int. J. Pharm. (2021), https://doi.org/10.1016/j.ijpharm.2021.120381.

[35] G.T. Hermanson, Bioconjugate Techniques, Third Edition, 2013, https://doi.org/10.1016/C2009-0-64240-9.

[36] D.P. Nair, M. Podgórski, S. Chatani, T. Gong, W. Xi, C.R. Fenoli, C.N. Bowman, The Thiol-Michael addition click reaction: a powerful and widely used tool in materials chemistry, Chem. Mater. (2014), https://doi.org/10.1021/cm402180t.

[37] M. Oswald, S. Geissler, A. Goepferich, Determination of the activity of maleimide-functionalized phospholipids during preparation of liposomes, Int. J. Pharm. (2016), https://doi.org/10.1016/j.ijpharm.2016.06.116.

[38] D.L. Iden, T.M. Allen, In vitro and in vivo comparison of immunoliposomes made by conventional coupling techniques with those made by a new post-insertion approach, Biochim. Biophys. Acta Biomembr. (2001), https://doi.org/10.1016/S0005-2736(01)00357-1.

[39] K. Laginha, D. Mumbengegwi, T. Allen, Liposomes targeted via two different antibodies: assay, B-cell binding and cytotoxicity, Biochim. Biophys. Acta Biomembr. (2005), https://doi.org/10.1016/j.bbamem.2005.02.007.

[40] A.A. Sağıroğlu, Y. Özsoy, Ö. Özer, Design, optimization and characterization of novel topical formulations containing Triamcinolone Acetonide, J. Drug Deliv. Sci. Technol. (2020), https://doi.org/10.1016/j.jddst.2020.101594.

[41] S. Amselem, E. Zawoznik, A. Yogev, D. Friedman, EmulsomesTM, a new type of lipid assembly, in: Handb. Nonmedical Appl. Liposomes Vol. III from Des. To Microreactors, 2018, https://doi.org/10.1201/9781351072724.

[42] M.H. Ucisik, S. Küpcü, A. Breitwieser, N. Gelbmann, B. Schuster, U.B. Sleytr, S-layer fusion protein as a tool functionalizing emulsomes and CurcuEmulsomes for antibody binding and targeting, Colloids Surf. B Biointerfaces 128 (2015) 132–139, https://doi.org/10.1016/j.colsurfb.2015.01.055.

[43] I. Steinhauser, B. Spänkuch, K. Strebhardt, K. Langer, Trastuzumab-modified nanoparticles: optimisation of preparation and uptake in cancer cells, Biomaterials (2006), https://doi.org/10.1016/j.biomaterials.2006.05.016.

[44] L. Talarico, S. Pepi, S. Susino, G. Leone, C. Bonechi, M. Consumi, I. Clemente, A. Magnani, Design and optimization of solid lipid nanoparticles loaded with triamcinolone acetonide, Molecules (2023), https://doi.org/10.3390/molecules28155747.

[45] M. Ucisik, U. Sleytr, B. Schuster, Emulsomes meet S-layer proteins: an emerging targeted drug delivery system, Curr. Pharmaceut. Biotechnol. 16 (2015) 392–405, https://doi.org/10.2174/1389201016041502181126 56.

[46] S.P. Vyas, R. Subhedar, S. Jain, Development and characterization of emulsomes for sustained and targeted delivery of an antiviral agent to liver, J. Pharm. Pharmacol. (2006), https://doi.org/10.1211/jpp.58.3.0005.

[47] M.S. Webb, T.O. Harasym, D. Masin, M.B. Bally, L.D. Mayer, Sphingomyelin-cholesterol liposomes significantly enhance the pharmacokinetic and therapeutic properties of vincristine in murine and human tumour models, Br. J. Cancer (1995), https://doi.org/10.1038/bjc.1995.430.

[48] A. Chinsriwongkul, Development of Lipid Nanoparticles for Anticancer Drug Delivery Systems, Silpakorn University, 2009. http://www.sure.su.ac.th/xmlui/bitstream/handle/123456789/12739/Fulltext.pdf?sequence=1&isAllowed=y.
[49] H. Heiati, R. Tawashi, N.C. Phillips, Drug retention and stability of solid lipid nanoparticles containing azidothymidine palmitate after autoclaving, storage and lyophilization, J. Microencapsul. (1998), https://doi.org/10.3109/02652049809006847.
[50] M. Danaei, M. Dehghankhold, S. Ataei, F. Hasanzadeh Davarani, R. Javanmard, A. Dokhani, S. Khorasani, M.R. Mozafari, Impact of particle size and polydispersity index on the clinical applications of lipidic nanocarrier systems, Pharmaceutics (2018), https://doi.org/10.3390/pharmaceutics10020057.
[51] X. Chen, Z. Zhang, S. Yang, H. Chen, D. Wang, J. Li, All-trans retinoic acid-encapsulated, CD20 antibody-conjugated poly(Lactic-co-glycolic acid) nanoparticles effectively target and eliminate melanoma-initiating cells in vitro, OncoTargets Ther. (2018), https://doi.org/10.2147/OTT.S169957.
[52] B.S. Zolnik, Á. González-Fernández, N. Sadrieh, M.A. Dobrovolskaia, Minireview: nanoparticles and the immune system, Endocrinology (2010), https://doi.org/10.1210/en.2009-1082.
[53] A. Albanese, W.C.W. Chan, Effect of gold nanoparticle aggregation on cell uptake and toxicity, ACS Nano (2011), https://doi.org/10.1021/nn2007496.
[54] J. Cai, Y. Yue, D. Rui, Y. Zhang, S. Liu, C. Wu, Effect of chain length on cytotoxicity and endocytosis of cationic polymers, Macromolecules (2011), https://doi.org/10.1021/ma102498g.
[55] H. Lv, S. Zhang, B. Wang, S. Cui, J. Yan, Toxicity of cationic lipids and cationic polymers in gene delivery, J. Contr. Release (2006), https://doi.org/10.1016/j.jconrel.2006.04.014.
[56] A. Magarkar, V. Dhawan, P. Kallinteri, T. Viitala, M. Elmowafy, T. Róg, A. Bunker, Cholesterol level affects surface charge of lipid membranes in saline solution, Sci. Rep. (2014), https://doi.org/10.1038/srep05005.
[57] O.K. Nag, V. Awasthi, Surface engineering of liposomes for stealth behavior, Pharmaceutics (2013), https://doi.org/10.3390/pharmaceutics5040542.
[58] M. Pereira, E.P.C. Lai, Capillary electrophoresis for the characterization of quantum dots after non-selective or selective bioconjugation with antibodies for immunoassay, J. Nanobiotechnol. (2008), https://doi.org/10.1186/1477-3155-6-10.
[59] J.N. Moreira, T. Ishida, R. Gaspar, T.M. Allen, Use of the post-insertion technique to insert peptide ligands into pre-formed stealth liposomes with retention of binding activity and cytotoxicity, Pharm. Res. (N. Y.) (2002), https://doi.org/10.1023/A:1014434732752.
[60] T. Ishida, D.L. Iden, T.M. Allen, A combinatorial approach to producing sterically stabilized (Stealth) immunoliposomal drugs, FEBS Lett. (1999), https://doi.org/10.1016/S0014-5793(99)01320-4.
[61] N. Dinauer, S. Balthasar, C. Weber, J. Kreuter, K. Langer, H. Von Briesen, Selective targeting of antibody-conjugated nanoparticles to leukemic cells and primary T-lymphocytes, Biomaterials (2005), https://doi.org/10.1016/j.biomaterials.2005.02.038.
[62] M. Kretschmar, S. Amselem, E. Zawoznik, K. Mosbach, A. Dietz, H. Hof, T. Nichterlein, Efficient treatment of murine systemic infection with Candida albicans using amphotericin B incorporated in nanosize range particles (emulsomes), Mycoses 44 (2001) 281–286, https://doi.org/10.1046/j.1439-0507.2001.00654.x.
[63] X.-J. Chen, X.-Q. Zhang, M.-X. Tang, G. Zhou, PD-l1 conjugated all-trans retinoic acid nanoparticles for targeted treatment of oral dysplasia and oral squamous cell carcinoma, Oral Surg. Oral Med. Oral Pathol. Oral Radiol. (2020), https://doi.org/10.1016/j.oooo.2019.07.059.